



CERN-EP-2023-191
29 August 2023

Probing the Chiral Magnetic Wave with charge-dependent flow measurements in Pb–Pb collisions at the LHC

ALICE Collaboration*

Abstract

The Chiral Magnetic Wave (CMW) phenomenon is essential to provide insights into the strong interaction in QCD, the properties of the quark–gluon plasma, and the topological characteristics of the early universe, offering a deeper understanding of fundamental physics in high-energy collisions. Measurements of the charge-dependent anisotropic flow coefficients are studied in Pb–Pb collisions at center-of-mass energy per nucleon–nucleon collision $\sqrt{s_{NN}} = 5.02$ TeV to probe the CMW. In particular, the slope of the normalized difference in elliptic (v_2) and triangular (v_3) flow coefficients of positively and negatively charged particles as a function of their event-wise normalized number difference, is reported for inclusive and identified particles. The slope r_3^{Norm} is found to be larger than zero and to have a magnitude similar to r_2^{Norm} , thus pointing to a large background contribution for these measurements. Furthermore, r_2^{Norm} can be described by a blast wave model calculation that incorporates local charge conservation. In addition, using the event shape engineering technique yields a fraction of CMW (f_{CMW}) contribution to this measurement which is compatible with zero. This measurement provides the very first upper limit for f_{CMW} , and in the 10–60% centrality interval it is found to be 26% (38%) at 95% (99.7%) confidence level.

arXiv:2308.16123v1 [nucl-ex] 30 Aug 2023

1 Introduction

The primary goal of relativistic heavy-ion collisions at the Large Hadron Collider (LHC) is to study the properties of the emerging strongly interacting medium called the quark–gluon plasma (QGP) [1–6]. The transition from normal hadronic matter to the QGP is predicted by quantum chromodynamics (QCD) calculations on the lattice [7, 8]. Heavy-ion collisions are also characterized by extremely strong short-lived electromagnetic fields ($B \sim 10^{18}$ Gauss), primarily induced by protons from the incoming nuclei that do not undergo any inelastic collision and are referred to as spectators [9]. The direction of \mathbf{B} is perpendicular to the reaction plane, the plane spanned by the impact parameter of the colliding nuclei and the beam direction. The presence of this intense magnetic field allows for the possibility to study novel QCD phenomena, such as parity violation in strong interactions [10–12].

The potential to observe parity violation in strong interactions using ultrarelativistic heavy-ion collisions was first discussed in Refs. [12–14] and further reviewed in Refs. [15–18]. Theoretically, the interactions of quarks with gluonic fields describing transitions between topologically different QCD vacuum states change the quark chirality, leading to a local chiral imbalance. The strong magnetic field leads to a charge separation (electric current) relative to the reaction plane, which is known as the Chiral Magnetic Effect (CME) [12, 19–22]. The experimental search for the CME using heavy-ion collisions has intensified over the past decade. Though early measurements pointed to some similarities between the results and the theoretical predictions [23–25], there is substantial evidence that background sources, i.e., collective phenomena and local charge conservation (LCC), play a significant role in the experimental measurements [26, 27]. The LCC here refers to the principle that within a local region of a physical system, the balance or conservation of quantum numbers for eg., electric charge is upheld. Experimental results indicate that the upper limit of the CME signal contribution ranges from 7% to 20% at 95% confidence level in semicentral heavy-ion collisions [23–35].

A dual phenomenon to the CME is the Chiral Separation Effect (CSE) [36, 37], which is theorized to induce a chirality current along \mathbf{B} in the presence of a finite electric chemical potential (μ_e). The CME and the CSE interact with one another forming a long wavelength collective excitation, called the Chiral Magnetic Wave (CMW) [38–42]. Similar to the CME-induced electric dipole moment, the CMW would manifest itself in a finite electric quadrupole moment in the final state [38]. This effect, if present, can be measured by charge-dependent anisotropic flow measurements [38]. The anisotropic flow is quantified in terms of the Fourier coefficients v_n of the azimuthal distribution of the produced particles with respect to the n^{th} -order event plane angle Ψ_n [43, 44]

$$\frac{dN}{d\varphi} \propto 1 + \sum_{n=1}^{\infty} 2v_n \cos[n(\varphi - \Psi_n)], \quad (1)$$

where φ is the azimuthal angle of a particle. The first three coefficients v_1 , v_2 , and v_3 are known as the directed, elliptic, and triangular flow, respectively. The CMW-induced electric quadrupole moment evolves with the medium expansion, leading to an increase (decrease) of v_2 for negatively (positively) charged hadrons [38]. The difference between negatively and positively charged hadron v_2 (Δv_2) is expected to be proportional to the event-by-event charge asymmetry (A_{ch}) [38, 39],

$$\Delta v_2 = v_2^- - v_2^+ \propto r_2 A_{\text{ch}}. \quad (2)$$

In the above equation, r_2 denotes the slope parameter between Δv_2 and event-by-event charge asymmetry, and A_{ch} is defined as

$$A_{\text{ch}} = \frac{(N^+ - N^-)}{(N^+ + N^-)}, \quad (3)$$

where N^+ (N^-) are positively (negatively) charged hadrons measured in a given event.

The first experimental search for the CMW was performed by the STAR Collaboration at the Relativistic Heavy Ion Collider (RHIC) with charged pions in Au–Au collisions at center-of-mass energy per

nucleon–nucleon collision $\sqrt{s_{\text{NN}}} = 200$ GeV [45], in which a positive linear dependence on A_{ch} was observed for the v_2 difference between π^- and π^+ . The extracted positive slopes as well as their centrality dependence agree well with theoretical calculations [38–40]. A similar positive correlation was measured by the ALICE Collaboration at the Large Hadron Collider (LHC) with charged hadrons in semicentral Pb–Pb collisions at $\sqrt{s_{\text{NN}}} = 2.76$ TeV [46]. Comparable slopes to those from Au–Au collisions in semicentral collisions were reported. However, the lifetime of the magnetic field in vacuum is expected to drop much faster at LHC energies compared to that at RHIC energies [47]. Thus, it is highly unlikely that an identical slope value would be observed by different experiments with orders of magnitude difference in collision energies. Furthermore, a similar linear dependence was observed by the precision measurements of the CMS collaboration in p–Pb and Pb–Pb collisions at $\sqrt{s_{\text{NN}}} = 5.02$ TeV [48]. This similarity questioned the CMW interpretation since the CMW signal is not expected to be present in p–Pb collisions due to the decoupling of the magnetic field from the reaction plane in such collisions [32, 49]. In addition, both STAR and CMS collaborations have observed a linear dependence between A_{ch} and Δv_3 , i.e. the difference between the v_3 coefficients of negatively and positively charged hadrons [48, 50]

$$\Delta v_3 = v_3^- - v_3^+ \propto r_3 A_{\text{ch}}. \quad (4)$$

However, this should not originate from the CMW-induced electric quadrupole configuration in the medium as the CMW is mainly driven by the magnetic field which is uncorrelated with the third order event plane. As a result of these observations, it appears likely that the slope observed in Δv_2 as a function of A_{ch} is not due to the CMW processes only. To ease the comparison between measurements performed by different experiments, one can define a normalized slope parameter as,

$$\Delta v_n^{\text{Norm}} = \frac{v_n^- - v_n^+}{(v_n^- + v_n^+)/2} \propto r_n^{\text{Norm}} A_{\text{ch}}, \quad (5)$$

where $n = 2$ or 3 . Recently, it was proposed in Ref. [51], that one can also utilize the event shape engineering (ESE) technique [35] to estimate the CMW signal. This selection methodology was already employed to constrain the CME [31, 34]. The ESE approach utilizes the fluctuations in the shape of the initial state of the system and allows one to select events with the same centrality but different initial geometry, thus varying the background contributions. Instead of the $A_{\text{ch}}-v_2$ slope, an alternative observable, the integral covariance [46] can be used. It is defined as

$$\Delta \text{IC} = \left(\langle v_2^- A_{\text{ch}} \rangle - \langle A_{\text{ch}} \rangle \langle v_2^- \rangle \right) - \left(\langle v_2^+ A_{\text{ch}} \rangle - \langle A_{\text{ch}} \rangle \langle v_2^+ \rangle \right), \quad (6)$$

where the angular bracket denotes the average over the events. This observable, by definition, calculates the covariance between A_{ch} and v_2 and is equivalent to the slope parameter. The main advantage of such a covariance is the removal of the dependence on the detector acceptance and on the reconstruction efficiency of charged hadrons [46]. In addition, one no longer needs to divide each sub-sample of v_2 into several A_{ch} intervals allowing for a reduction of the statistical fluctuations.

Understanding the background components and how they contribute to the experimental measurements is crucial to isolate the CMW signal. Among several background sources [52–59], the most dominant one is expected to be the LCC, convoluted with the collective motion of the QGP medium. The LCC mechanism depicts a scenario where pairs of particles with opposite charges are usually generated from resonance decays. Such particle production mechanism is studied with balance function measurements in heavy-ion collisions [60, 61]. In the CMW measurement, when one of the particles from the charge-conserving pair escapes from the limited detector acceptance, a non-zero A_{ch} is consequently generated [52]. It is demonstrated in Ref. [62] that the selection of specific A_{ch} values automatically biases the $\eta-p_{\text{T}}$ phase space. This can trivially give rise to a $A_{\text{ch}}-\Delta v_2$ correlation because of the v_2 dependence on η and p_{T} leading to non-zero slopes, even in absence of CMW phenomena. Theoretical studies on $A_{\text{ch}}-\Delta v_2$ correlations, without the CMW process, have been extensively investigated in Refs. [63–67]. The

consensus is that the LCC interpretation can effectively explain both the observed $A_{\text{ch}}-\Delta v_3$ and $A_{\text{ch}}-\Delta v_2$ relations. A pure LCC mechanism is expected to lead to a similar positive linear correlation between $A_{\text{ch}}-\Delta v_2^{\text{Norm}}$ and $A_{\text{ch}}-\Delta v_3^{\text{Norm}}$. Consequently, this implies that any difference between the normalized slopes r_2^{Norm} and r_3^{Norm} may indicate the existence of the CMW signal.

Although there are several measurements of CMW at LHC energies, there is lack of measurements with identified hadrons. Given that the predominant background influence on CMW arises from the interplay of LCC and elliptic flow (v_2), it would be useful to measure the CMW for identified particles, as it would provide us a better handle to control the background related to v_2 [38]. The first theoretical study [38] predicted that only light quarks, i.e., u and d, are influenced by the chiral anomaly. However, recent theoretical calculations [68] suggest that the mass difference between the strange quark (s) and the u, d quarks can be neglected, indicating the possibility of exploring CMW effects with charged kaons. Nevertheless, the significant differences in the absorption cross section for (anti-)protons and kaons in the hadronic matter might obscure the signal. Additionally, a hydrodynamic study [56] suggests that the isospin chemical potential (μ_I) and the strangeness chemical potential (μ_S) can play essential roles. This study predicts a negative slope for kaons at RHIC energies [56]. Therefore, it is difficult to disentangle the CMW signal and various background contributions, if the measurements are performed only with inclusive charged hadrons.

This paper presents the first measurement of normalized slopes r_2^{Norm} and r_3^{Norm} for charged hadrons and identified π^\pm , K^\pm , and $p+\bar{p}$ in Pb–Pb collisions at $\sqrt{s_{\text{NN}}} = 5.02$ TeV. These measurements will provide experimental input to the ongoing theoretical developments for the flavor dependence of the chiral anomalies. Measurements from data are further compared with a recently developed blast wave model calculation, incorporating the LCC background (BW+LCC) [69]. The measurement of integral covariance is also utilized to estimate an upper limit on the CMW contribution, for the first time, in Pb–Pb collisions at $\sqrt{s_{\text{NN}}} = 5.02$ TeV.

This article is organized as follows: Section 2 briefly describes the experimental setup, while Section 3 discusses the data sample, the selection criteria, and the analysis details. Section 4 describes the evaluation of the systematic uncertainties. The results are discussed and compared with model calculations in Section 5. A summary is outlined in Section 6.

2 Experimental apparatus and data sample

The ALICE detector and its performance are described in detail in Refs. [70, 71]. The apparatus consists of a central barrel at midrapidity ($|\eta| < 0.9$), embedded in a cylindrical solenoid which provides a magnetic field of 0.5 T parallel to the beam direction, and a set of forward detectors.

Charged particles produced in the collisions at midrapidity are tracked by the Inner Tracking System (ITS) [70] and the Time Projection Chamber (TPC) [72]. The ITS, composed of the Silicon Pixel Detector (SPD), Silicon Drift Detector (SDD), and Silicon Strip Detector (SSD), consists of six cylindrical silicon layers surrounding the beam vacuum pipe. The TPC, surrounding the ITS, provides up to 159 points for track reconstruction along with specific energy loss (dE/dx) measurements, which are utilized for charged-particle identification (PID). The PID is complemented by a Time-Of-Flight (TOF) detector [73], which measures the flight time of charged particles. The TOF detector provides pion–kaon separation at 3σ level up to $p_T \simeq 2.5$ GeV/ c and pion–proton separation up to $p_T \simeq 4$ GeV/ c .

On either sides of the interaction point, the V0 scintillator arrays [74], are used for triggering and event classification. The V0 detector consists of two arrays of 32 scintillator tiles covering the pseudorapidity ranges $2.8 < \eta < 5.1$ (V0A) and $-3.7 < \eta < -1.7$ (V0C). Both V0 detectors are segmented in four rings in the radial direction with each ring divided into eight sectors in the azimuthal direction. The V0C is also used for ESE and event selection. Two tungsten-quartz neutron Zero Degree Calorimeters

(ZDCs) [70], positioned 112.5 meters from the interaction point on each side, are used to reduce the contamination from beam-induced background. Using the time information from V0 and ZDC, offline event selection is performed to reject background from beam–gas collisions, from parasitic beam–beam interactions, and pileup events [71, 75].

The analysis is performed using the data sample collected with the ALICE apparatus in the 2018 LHC Pb–Pb run at $\sqrt{s_{NN}} = 5.02$ TeV. The centrality intervals were defined in terms of percentiles of the hadronic Pb–Pb cross section, determined from selections on the sum of the V0 signal amplitudes [76]. Central and semicentral Pb–Pb collisions were selected online by applying thresholds on the V0 signal amplitudes resulting in two separate trigger classes (central and semicentral triggers).

Only events with a reconstructed primary vertex located between ± 10 cm with respect to the nominal interaction point along the beam direction (z axis of the ALICE reference frame) are considered. The analysis is performed in different centrality intervals spanning from 0–5% which corresponds to the most central collisions to 50–60% corresponding to peripheral collisions. The total number of analyzed events after the event selection is approximately 240 million.

3 Analysis procedure

Charged particles reconstructed using the TPC and the ITS information within $|\eta| < 0.8$ and $0.2 < p_T < 10$ GeV/ c are considered to determine A_{ch} . For the measurement of flow coefficients, charged particles are restricted to $0.2 < p_T < 2.0$ GeV/ c . Tracks are selected requiring $|\eta| < 0.8$, at least 70 (out of a maximum of 159) TPC space points, and χ^2 per TPC cluster < 2.5 for the momentum fit in the TPC. In order to reduce the contamination from secondary particles (i.e., particles originating from weak decays, conversions, and secondary hadronic interactions in the detector material) only tracks with a maximum distance of closest approach (DCA) to the reconstructed primary vertex in the transverse ($|DCA_{xy}| < 2.4$ cm) and the longitudinal directions ($|DCA_z| < 3.2$ cm) are accepted. Furthermore, tracks are required to have at least one hit in the two SPD layers. Charged pions, kaons, and (anti)protons are identified from the difference between the measured and expected values of dE/dx in TPC and time of flight to the TOF detector, expressed in units of resolution ($|n\sigma|_{TPC}$, $|n\sigma|_{TOF}$), and applying a selection on the number of accepted $n\sigma$ (see Table 1). Additionally, tracks without TOF information with p_T larger than 0.5 GeV/ c for pions, 0.45 GeV/ c for kaons, and 0.6 GeV/ c for protons are rejected. All particle species are required to lie within the rapidity range $|y| < 0.5$. By applying these selection criteria, the efficiency of identifying charged hadrons is approximately 70% around $p_T = 0.5$ GeV/ c and increases to about 80% for p_T values above 1 GeV/ c . Moreover, these selection criteria guarantee a purity exceeding 90% for all particle species across the entire range of p_T values considered in the analysis.

An example of the measured raw A_{ch} distribution is shown in the left panel of Fig. 1 for the 40–50% centrality interval. The raw A_{ch} distribution is divided into ten A_{ch} intervals, each roughly containing equal number of events. The edges of the ten A_{ch} classes are displayed by the dashed lines in the left panel of Fig. 1. The raw A_{ch} is corrected to account for the limited detector acceptance and the reconstruction and identification efficiency of charged hadrons. Using simulations based on the HIJING event generator [77] combined with the GEANT3 model [78] for particle transport in the detector material, a correlation is built between the raw and the true values of A_{ch} [50]. A linear fit to this correlation is performed and the fit function is used to map the raw A_{ch} to the true A_{ch} as shown in the right panel of Fig. 1.

Within each A_{ch} interval, the flow coefficients v_2 and v_3 are measured separately for positively and negatively (identified and inclusive) charged hadrons. The measurements are performed using the two-particle cumulant method [79] with a pseudorapidity gap of $|\Delta\eta| > 0.4$ to suppress non-flow, i.e. correlations not related to the reaction plane [80]. The normalized slope parameters, r_2^{Norm} and r_3^{Norm} , are then calculated for various centrality intervals with Eq. 5 using the values of A_{ch} corrected for detector effects as

described above.

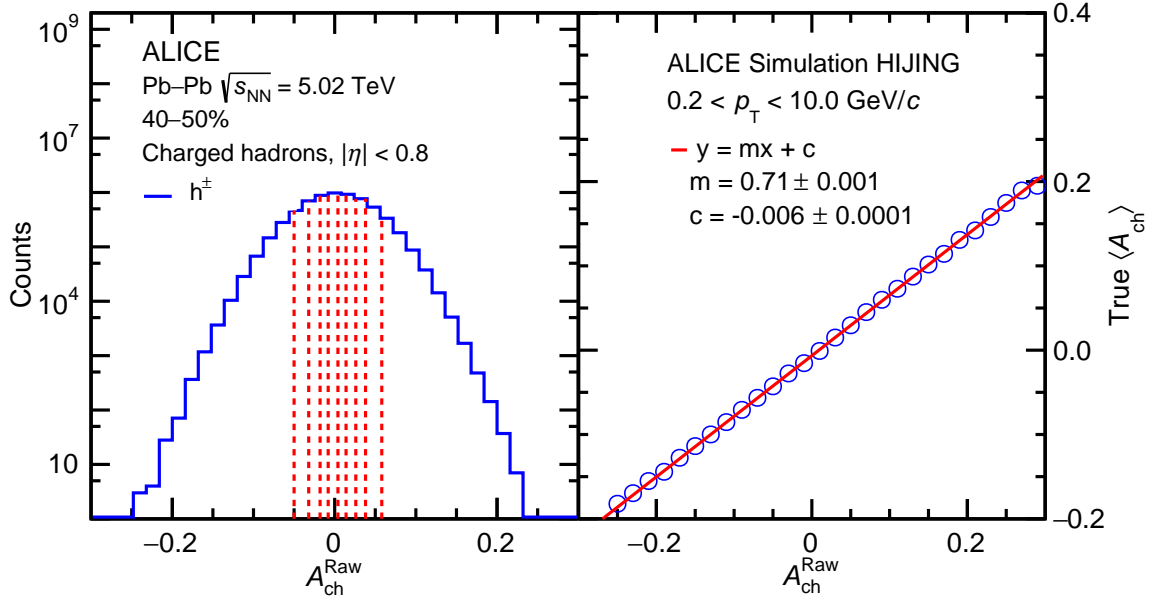


Figure 1: (Left panel): Raw A_{ch} distribution in Pb–Pb collisions at $\sqrt{s_{\text{NN}}} = 5.02$ TeV for the 40–50% centrality interval. Red dotted lines depict the edges of the ten A_{ch} classes. (Right panel): Correlation between true and raw A_{ch} obtained from HIJING simulations combined with a GEANT3 detector model for Pb–Pb collisions at $\sqrt{s_{\text{NN}}} = 5.02$ TeV in the 40–50% centrality interval.

The ESE technique is further employed to estimate possible CMW signal contribution to the ΔIC as proposed in Ref. [51]. In particular, the residual magnitude of this observable when v_2 goes to zero can be used to disentangle the potential CMW signal from the background contributions [31]. The second-order reduced flow vector q_2 is used for event shape selection as in Ref. [31]. It is defined as

$$q_2 = Q_2 / \sqrt{M}, \quad (7)$$

where Q_2 is the magnitude of the flow vector and M is the multiplicity. The Q_2 is calculated from the azimuthal distribution of the energy deposited in the V0C detector. In order to account for a non-uniform detector response, the V0 detector is calibrated using two procedures: gain equalization and recentering. The former flattens the mean multiplicity distribution of the eight azimuthal sectors in each ring, while the latter corrects for systematic shifts of the mean values of the Q_2 vector components [44]. For each centrality interval, ten q_2 ranges are explored, ranging from the most elliptic to the most isotropic event classes.

To separate the LCC background contributions from the potential CMW signal, the dependence of the ΔIC on v_2 (defined in Section 1) is fitted with a linear function. The CMW fraction to the ΔIC is then obtained by the ratio between the observable at zero v_2 and at finite v_2

$$f_{\text{CMW}} \equiv \frac{b}{a \langle v_2 \rangle + b}, \quad (8)$$

where a and b are the slope and the intercept of the linear function, respectively, and $\langle v_2 \rangle$ is the average value over the measured v_2 range.

4 Systematic uncertainties

To estimate the systematic uncertainties on the normalized slopes and f_{CMW} , the event and track selection criteria are varied from their nominal values. Table 1 provides a list of variables used in the selections along with their default and varied values. These include modifying the range of z coordinate of the primary vertex (V_z) from $|V_z| \leq 10$ cm to $|V_z| \leq 8$ cm to examine the detector acceptance dependence. The impact of the track-quality selections is evaluated by changing the minimum number of TPC space points from 70 to 80 and varying the χ^2_{TPC} per TPC space point from 2.5 to 2.0. To test the influence of the contamination from secondary particles on the measurement, tighter selection criteria than the nominal ones are applied to both DCA_{xy} and DCA_z . To estimate the effects of non-flow contributions, the pseudorapidity gap ($\Delta\eta$) is varied from $|\Delta\eta| \geq 0.4$ to $|\Delta\eta| \geq 0.6$ for charged hadrons and pions, and to $|\Delta\eta| \geq 0.5$ for kaons and protons. Particle identification criteria, namely $|n\sigma|_{\text{TPC}}$ and $|n\sigma|_{\text{TOF}}$, are also subject to variations to account for potential systematic effects in the particle identification process and their impact on the final analysis results. The reconstruction efficiency for charged hadrons is calculated using only pions, kaons, and protons and the differences observed in the results are incorporated as systematic uncertainties. For each systematic variation, the corrections for the non-uniform acceptance and for the reconstruction efficiency of inclusive and identified charged hadrons are estimated using collision data and MC simulations. To identify the statistically significant systematic sources, the ratio $B = Y/\sigma_B$ is calculated, where Y represents the difference between the results with the default and the modified selections, and σ_B is the error of the difference estimated as $\sqrt{|\sigma_{\text{default}}^2 \pm \sigma_{\text{varied}}^2|}$, where “+” is used for the uncorrelated and “-” for the correlated sources. The statistical uncertainties σ_{default} and σ_{varied} are estimated separately for the results using the default and varied event/particle selection criteria, following a subsampling method, with 20 equally sized independent samples. Each variation that exhibits a significant difference from the nominal result by more than $1\sigma_B$, according to the recommendations from Ref. [81], is considered a source of systematic uncertainty. The total systematic uncertainties are then obtained by summing the different contributions in quadrature.

Table 1: Nominal event and track selection criteria and the corresponding variations used for the estimation of the systematic uncertainties.

(No.) Source	Default Value	Variations
(1) Primary $ V_z $	< 10 cm	< 8 cm
(2) TPC space points	> 70	> 80
(3) $\chi^2_{\text{TPC}}/\text{cluster}$	< 2.5	< 2.0
(4) DCA_{xy} (DCA_z)	< 2.4 (3.2) cm	< 7(0.0026 + (0.005/ $p_T^{1.01}$)), (2.0) cm
(5) $ \Delta\eta $	> 0.4	> 0.6 (0.5 for K and p)
(6) PID (π)	-	-
0.2 < p_T < 0.5 (Gev/c)	$ n\sigma _{\text{TPC}} < 3$	$ n\sigma _{\text{TPC}} < 2.5$
0.5 < p_T < 2.0 (Gev/c)	$\sqrt{ n\sigma _{\text{TPC}}^2 + n\sigma _{\text{TOF}}^2} < 3$	$\sqrt{ n\sigma _{\text{TPC}}^2 + n\sigma _{\text{TOF}}^2} < 3$
PID (K)	-	-
0.2 < p_T < 0.45 (Gev/c)	$ n\sigma _{\text{TPC}} < 3$	$ n\sigma _{\text{TPC}} < 2.5$
0.45 < p_T < 2.0 (Gev/c)	$\sqrt{ n\sigma _{\text{TPC}}^2 + n\sigma _{\text{TOF}}^2} < 2.5$	$\sqrt{ n\sigma _{\text{TPC}}^2 + n\sigma _{\text{TOF}}^2} < 2$
PID (p)	-	-
0.4 < p_T < 0.6 (Gev/c)	$ n\sigma _{\text{TPC}} < 3$	$ n\sigma _{\text{TPC}} < 3.5$
0.6 < p_T < 2.0 (Gev/c)	$\sqrt{ n\sigma _{\text{TPC}}^2 + n\sigma _{\text{TOF}}^2} < 3.0$	$\sqrt{ n\sigma _{\text{TPC}}^2 + n\sigma _{\text{TOF}}^2} < 3.5$
(7) Efficiency calculation	All unidentified charged hadrons	Identified charged hadrons (π +K+p)

Tables 2 summarizes the maximum magnitude of the systematic uncertainties on the normalized slopes

over all the centrality intervals from each individual source which passes the criteria described above. The systematic sources for the f_{CMW} observable are only a few, namely Primary V_z , $\chi_{\text{TPC}}^2/\text{cluster}$, and DCA selections. The associated uncertainties are 0.024, 0.047, and 0.068, respectively.

Table 2: Maximum systematic uncertainty (absolute value) on normalized slope per particle species over all centrality intervals from individual sources (see Table 1 for an explanation of each source).

Sources	inclusive (h^\pm)		π^\pm		K^\pm		$p+\bar{p}$	
	r_2^{Norm}	r_3^{Norm}	r_2^{Norm}	r_3^{Norm}	r_2^{Norm}	r_3^{Norm}	r_2^{Norm}	r_3^{Norm}
(1) Primary V_z	0.014	0.03	0.012	0.03	0.019	0.12	0.02	0.021
(2) TPC space points	0.003	0.033	0.01	0.033	0.033	0.23	0.036	0.14
(3) $\chi_{\text{TPC}}^2/\text{cluster}$	0.009	0.047	0.0002	0.047	0.02	0.31	0.035	0.18
(4) DCA_{xy} (DCA_z)	0.005	0.044	0.023	0.044	0.02	0.18	0.026	0.19
(5) $ \Delta\eta $	0.013	0.09	0.018	0.09	0.017	0.31	0.052	0.11
(6) PID	-	-	0.05	0.05	0.013	0.11	0.004	0.13
(7) Efficiency	0.032	0.049	-	-	-	-	-	-

5 Results

5.1 A_{ch} dependence of v_n and centrality dependence of the slope r_n^{Norm}

The top left and top right panels of Fig. 2 show, respectively, the v_2 and v_3 of positively and negatively charged hadrons as a function of A_{ch} for Pb–Pb collisions at $\sqrt{s_{\text{NN}}} = 5.02$ TeV in the 40–50% centrality interval. A significant decreasing (increasing) trend of v_2 for positively (negatively) charged hadrons as a function of A_{ch} is observed. Such trends are also present for the v_3 coefficient though the fluctuations are larger. In Fig. 2 the correlated uncertainties between the hadrons and among A_{ch} intervals are represented with shaded bands. The normalized difference between the v_2 and v_3 of positive and negative charged particles, as defined in Eq. 5, is shown as a function of A_{ch} in the bottom left and right panels of Fig. 2, respectively. They are fitted with linear functions to obtain the slopes, r_2^{Norm} and r_3^{Norm} . In addition to a positive slope for $\Delta v_2/\langle v_2 \rangle$, a non-zero slope is also found for $\Delta v_3/\langle v_3 \rangle$ (i.e., $r_3^{\text{Norm}} > 0$), which mainly contains the background correlations. This non-zero r_3^{Norm} indicates that similar background is also present in r_2^{Norm} which need to be subtracted to make a quantitative measurement of CMW. Note that the difference in non-flow contributions to same-sign and opposite-sign pairs can induce a trivial correlation between v_n and A_{ch} [50, 82]. However, it is estimated that this trivial correlation is negligible at this collision energy. Figure 3 shows r_2^{Norm} (red markers) and r_3^{Norm} (green markers) as a function of centrality for inclusive charged hadrons in Pb–Pb collisions at $\sqrt{s_{\text{NN}}} = 5.02$ TeV. Despite the large uncertainties, r_3^{Norm} seems to be of similar magnitude to r_2^{Norm} , for most of the centrality range. The CMW is expected to develop in the direction of the magnetic field \mathbf{B} , i.e., approximately perpendicular to the second order event plane rather than the third order. The third order plane has very little correlation with the second order event plane [83–85]. Hence, the non-zero r_3^{Norm} value cannot originate from the CMW-induced electric quadrupole moment, but it should rather be attributed to the LCC mechanism. Thus, the similarity between the magnitudes of r_2^{Norm} and r_3^{Norm} could indicate that both of them are mainly dominated by the LCC background. The results are also in good agreement with the CMS measurements for the same collision system and energy [48]. While the precision of the CMS measurements is notable, the findings presented in this study expand the scope of measurements to encompass the most central collision scenarios. The r_2^{Norm} is further compared with a blast wave model calculation (green band) which takes into account the LCC effect [69]. This model uses blast wave parameters obtained from the simultaneous fit of p_{T} -differential yields and v_2 of identified particles from Pb–Pb collisions at $\sqrt{s_{\text{NN}}} = 5.02$ TeV [75]. Then, the model distributes source points within an ellipsoid (defined by the blast wave parameter) from where it produces oppositely charged particles (i.e. balancing charges). The number of sources is tuned in such a way that the A_{ch} distribution from the output of the model matches with the experimental data. Then, the normalized slope values are calculated from the model, following the

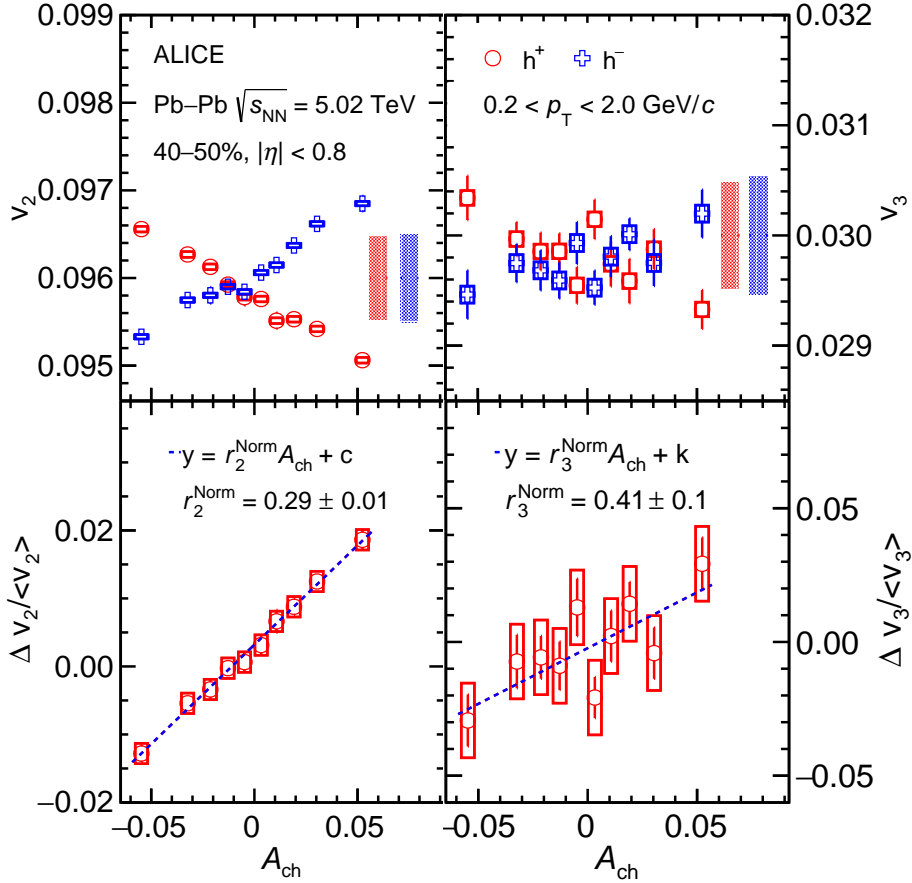


Figure 2: The top left panel shows the v_2 of positively (red markers) and negatively (blue markers) charged hadrons as a function of the corrected A_{ch} , while the top right panel shows the same for v_3 . Statistical uncertainties are shown by bars and uncorrelated (correlated) systematic uncertainties by open boxes (shaded bands). The bottom left panel shows $\Delta v_2 / \langle v_2 \rangle$ as a function of the corrected A_{ch} and bottom right panel shows the same for $\Delta v_3 / \langle v_3 \rangle$, all for the 40–50% centrality interval in Pb–Pb collisions at $\sqrt{s_{NN}} = 5.02$ TeV. The dotted blue line shows the linear fit to the data points to obtain the values of normalized slopes (r_2^{Norm} and r_3^{Norm}).

same procedure as in data. The agreement between the model and the experimental results of r_2^{Norm} points to a large background contribution in the measurement. The r_2^{Norm} and r_3^{Norm} results for identified hadrons are shown in Fig. 4 as a function of centrality. For r_2^{Norm} , the slope for kaons behaves similarly as the slope for pions, while the slope for protons slightly differs with a weak A_{ch} – Δv_2 dependence on centrality. In the 20% most central collisions, a hint of mass ordering is observed, i.e., the slopes of pions are slightly larger than those of kaons, and the slopes of kaons are slightly larger than those of protons. However, the uncertainties are too large for a definitive conclusion to be made. The LCC process, the dominant background for this measurement, can reproduce the measurement of r_2^{Norm} in data. Therefore, it is expected that the mass ordering of v_2 of identified particles might be the reason behind the apparent particle type dependence of r_2^{Norm} seen in Fig. 4. This finding contradicts the predictions of the hydrodynamic study, which anticipated negative slopes for kaons and protons [56]. A similar behavior is found in the STAR CMW measurement at a lower collision energy, in which the isospin and strangeness chemical potentials and the different absorption cross section are expected to play a role [50, 56, 86]. However, at LHC energies, the values of the chemical potentials are close to zero, suggesting that their influence should be negligible. For r_3^{Norm} , the slopes of all the measured hadron species are compatible with each other within the uncertainties. Since no predictions for the CMW for different particle species are available at LHC energies, the results shown here provide, for the first time, an experimental input

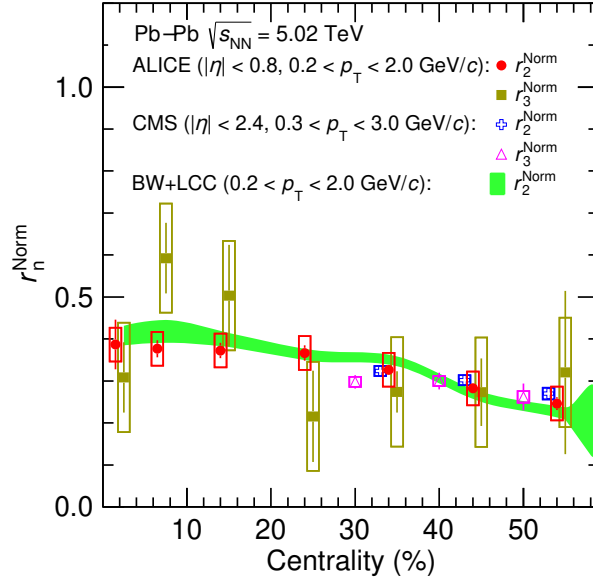


Figure 3: Centrality dependence of normalized slopes r_2^{Norm} and r_3^{Norm} for inclusive charged hadrons in Pb–Pb collisions at $\sqrt{s_{NN}} = 5.02$ TeV compared with CMS results [48] and a BW+LCC model calculation [69]. Statistical (systematic) uncertainties are depicted by bars (boxes). ALICE r_2^{Norm} and r_3^{Norm} and CMS r_2^{Norm} data points are slightly shifted horizontally for visibility.

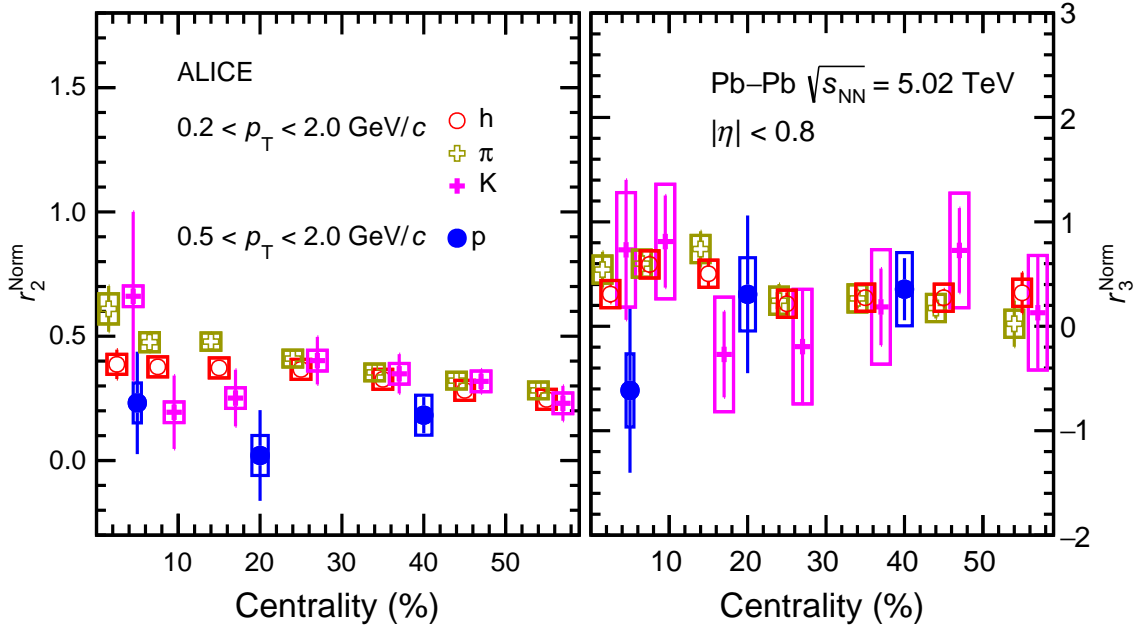


Figure 4: Centrality dependence of normalized slopes r_2^{Norm} (left panel) and r_3^{Norm} (right panel) for inclusive and identified charged hadrons in Pb–Pb collisions at $\sqrt{s_{NN}} = 5.02$ TeV. Statistical (systematic) uncertainties are depicted by bars (boxes). The data points for charged pions and kaons are slightly shifted horizontally for visibility.

for theoretical calculations.

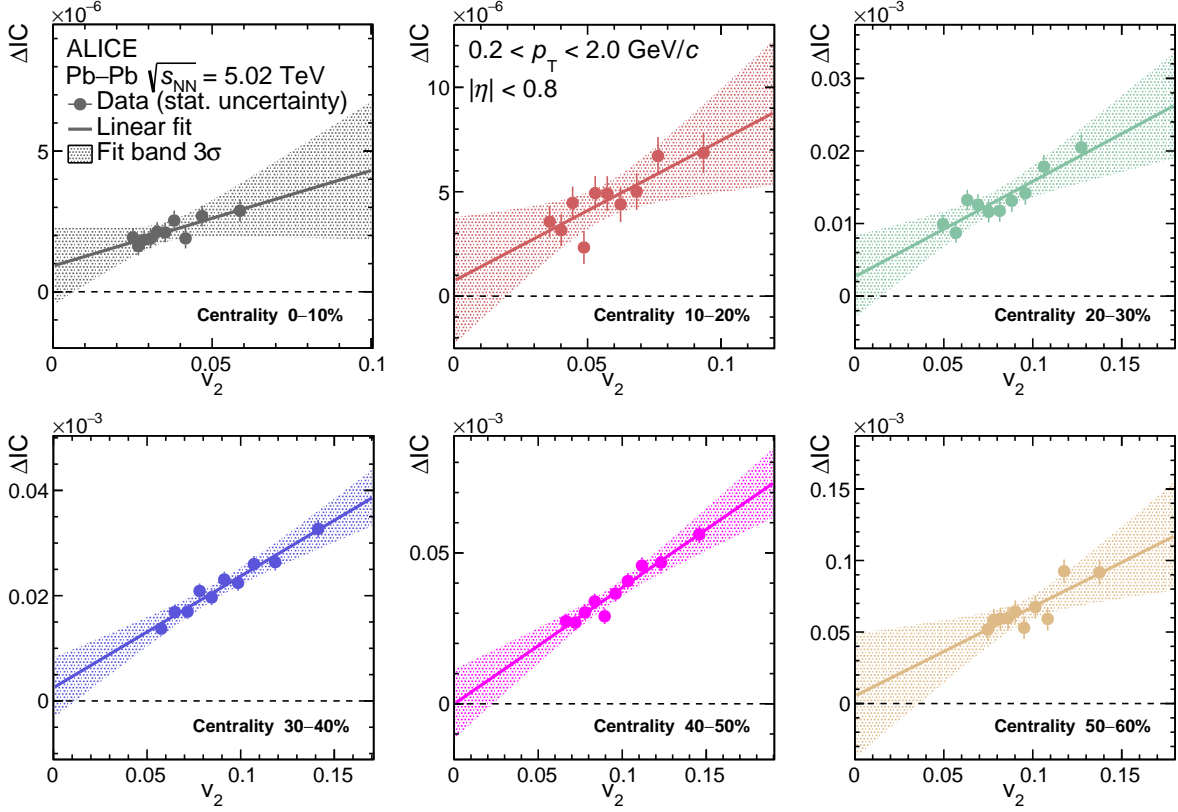


Figure 5: Dependence of ΔIC on v_2 of shape-selected events from the 0–10% (top left panel) to the 50–60% (bottom right panel) centrality intervals of Pb–Pb collisions at $\sqrt{s_{NN}} = 5.02$ TeV. The solid lines are straight line fit to the data points. Only statistical uncertainties are shown. The bands represent the three standard deviation uncertainties from the linear fit.

5.2 Constraining the fraction of the CMW with the ESE

Figure 5 shows the difference of the integrated covariance ΔIC as a function of v_2 for q_2 -selected events in six centrality intervals. Solid lines, representing linear fits, and colored bands, denoting three standard deviation uncertainties of the linear fits are also shown. The ΔIC values exhibit a decrease as v_2 approaches zero, as discussed in Ref. [51]. The small magnitude of the intercepts in all centrality intervals indicates that the measurement is dominated by the LCC background.

After obtaining the slope and intercept from the fit of ΔIC as a function of v_2 , the fraction of the CMW signal, denoted as f_{CMW} , can be determined using Eq. 8. The centrality dependence of f_{CMW} is presented in Fig. 6 where the error bars display the statistical uncertainties extracted from the fits of Fig. 5. Meaningful measurements are not possible in the most central and peripheral collisions, due to the small v_2 values and the large statistical fluctuations. Therefore, the f_{CMW} results are reported only in the 10–60% centrality range. The systematic uncertainties are estimated for the different possible sources, as discussed in Sec. 4. The systematic sources, which are found to be significant among centrality intervals, are combined in quadrature and shown as a dark shaded band in Fig. 6, at centrality around 60%. It is found that the f_{CMW} is consistent with zero within the reported statistical and systematic uncertainties.

The f_{CMW} data points in Fig. 6 are fitted with a constant, yielding a value of $f_{CMW} = 0.081 \pm 0.055$ (the dashed blue line), which should be combined with the systematic uncertainty of 0.087 (the gray box on the edge) to establish an upper limit on f_{CMW} of 26% (38%) at 95% (99.7%) confidence level shown by the dotted magenta line. This result provides the first quantitative assessment of the upper limit of the fraction of the Chiral Magnetic Wave (CMW) at the top LHC energy.

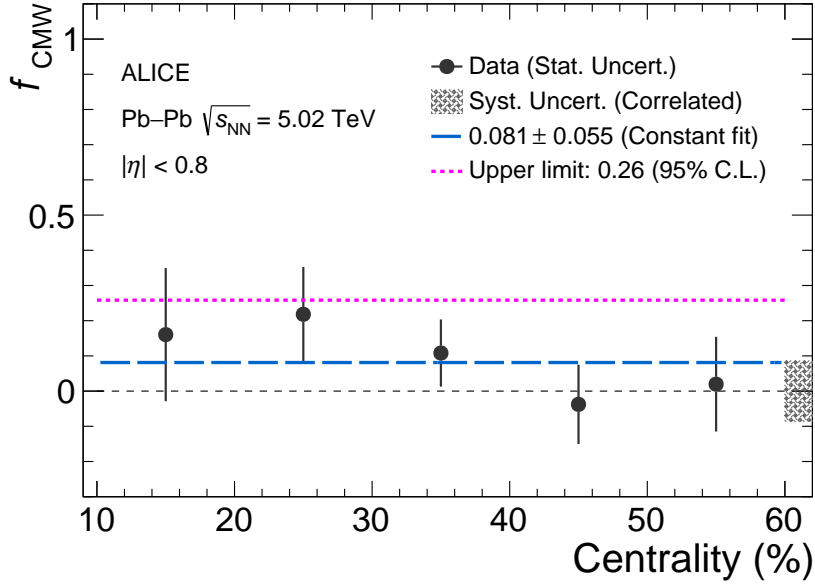


Figure 6: Centrality dependence of the extracted CMW fraction. The 95% confidence level of the upper limit is also shown by the dotted magenta line. Statistical uncertainties are depicted by bars, while the correlated systematic uncertainty is represented by a shaded band on the right edge. The blue line is the constant fit line of the data points.

6 Summary

The difference between the v_2 and v_3 coefficients of positively and negatively charged particles are measured as a function of the charge asymmetry A_{ch} for inclusive and identified hadrons in in Pb–Pb collisions at $\sqrt{s_{\text{NN}}} = 5.02$ TeV. The slopes r_2^{Norm} and r_3^{Norm} are found to be consistent with each other within the reported uncertainties, suggesting that the dominant contribution to r_2^{Norm} is not due to CMW. A blast wave parameterization that incorporates local charge conservation, tuned to reproduce the A_{ch} distribution, is able to fully describe the magnitude of r_2^{Norm} which is expected to be sensitive to CMW. Additionally, a hint for mass ordering of the r_2^{Norm} slopes of pions, kaons, and protons is discernible in the most central collisions, though it is accompanied by large uncertainties. Furthermore, using the Event Shape Engineering (ESE) technique, both the fraction and the upper limit of the CMW signal are extracted. Averaging over the 10–60% centrality interval, the CMW fraction is consistent with zero within uncertainties and an upper limit of 26% (38%) is estimated at 95% (99.7%) confidence level.

Acknowledgements

The ALICE Collaboration would like to thank all its engineers and technicians for their invaluable contributions to the construction of the experiment and the CERN accelerator teams for the outstanding performance of the LHC complex. The ALICE Collaboration gratefully acknowledges the resources and support provided by all Grid centres and the Worldwide LHC Computing Grid (WLCG) collaboration. The ALICE Collaboration acknowledges the following funding agencies for their support in building and running the ALICE detector: A. I. Alikhanyan National Science Laboratory (Yerevan Physics Institute) Foundation (ANSL), State Committee of Science and World Federation of Scientists (WFS), Armenia; Austrian Academy of Sciences, Austrian Science Fund (FWF): [M 2467-N36] and Nationalstiftung für Forschung, Technologie und Entwicklung, Austria; Ministry of Communications and High Technologies, National Nuclear Research Center, Azerbaijan; Conselho Nacional de Desenvolvimento Científico e Tecnológico (CNPq), Financiadora de Estudos e Projetos (Finep), Fundação de Amparo à Pesquisa do Estado de São Paulo (FAPESP) and Universidade Federal do Rio Grande do Sul (UFRGS),

Brazil; Bulgarian Ministry of Education and Science, within the National Roadmap for Research Infrastructures 2020–2027 (object CERN), Bulgaria; Ministry of Education of China (MOEC), Ministry of Science & Technology of China (MSTC) and National Natural Science Foundation of China (NSFC), China; Ministry of Science and Education and Croatian Science Foundation, Croatia; Centro de Aplicaciones Tecnológicas y Desarrollo Nuclear (CEADEN), Cubaenergía, Cuba; Ministry of Education, Youth and Sports of the Czech Republic, Czech Republic; The Danish Council for Independent Research | Natural Sciences, the VILLUM FONDEN and Danish National Research Foundation (DNRF), Denmark; Helsinki Institute of Physics (HIP), Finland; Commissariat à l’Energie Atomique (CEA) and Institut National de Physique Nucléaire et de Physique des Particules (IN2P3) and Centre National de la Recherche Scientifique (CNRS), France; Bundesministerium für Bildung und Forschung (BMBF) and GSI Helmholtzzentrum für Schwerionenforschung GmbH, Germany; General Secretariat for Research and Technology, Ministry of Education, Research and Religions, Greece; National Research, Development and Innovation Office, Hungary; Department of Atomic Energy Government of India (DAE), Department of Science and Technology, Government of India (DST), University Grants Commission, Government of India (UGC) and Council of Scientific and Industrial Research (CSIR), India; National Research and Innovation Agency - BRIN, Indonesia; Istituto Nazionale di Fisica Nucleare (INFN), Italy; Japanese Ministry of Education, Culture, Sports, Science and Technology (MEXT) and Japan Society for the Promotion of Science (JSPS) KAKENHI, Japan; Consejo Nacional de Ciencia (CONACYT) y Tecnología, through Fondo de Cooperación Internacional en Ciencia y Tecnología (FONCICYT) and Dirección General de Asuntos del Personal Académico (DGAPA), Mexico; Nederlandse Organisatie voor Wetenschappelijk Onderzoek (NWO), Netherlands; The Research Council of Norway, Norway; Commission on Science and Technology for Sustainable Development in the South (COMSATS), Pakistan; Pontificia Universidad Católica del Perú, Peru; Ministry of Education and Science, National Science Centre and WUT ID-UB, Poland; Korea Institute of Science and Technology Information and National Research Foundation of Korea (NRF), Republic of Korea; Ministry of Education and Scientific Research, Institute of Atomic Physics, Ministry of Research and Innovation and Institute of Atomic Physics and University Politehnica of Bucharest, Romania; Ministry of Education, Science, Research and Sport of the Slovak Republic, Slovakia; National Research Foundation of South Africa, South Africa; Swedish Research Council (VR) and Knut & Alice Wallenberg Foundation (KAW), Sweden; European Organization for Nuclear Research, Switzerland; Suranaree University of Technology (SUT), National Science and Technology Development Agency (NSTDA), Thailand Science Research and Innovation (TSRI) and National Science, Research and Innovation Fund (NSRF), Thailand; Turkish Energy, Nuclear and Mineral Research Agency (TENMAK), Turkey; National Academy of Sciences of Ukraine, Ukraine; Science and Technology Facilities Council (STFC), United Kingdom; National Science Foundation of the United States of America (NSF) and United States Department of Energy, Office of Nuclear Physics (DOE NP), United States of America. In addition, individual groups or members have received support from: European Research Council, Strong 2020 - Horizon 2020 (grant nos. 950692, 824093), European Union; Academy of Finland (Center of Excellence in Quark Matter) (grant nos. 346327, 346328), Finland.

References

- [1] W. Busza, K. Rajagopal, and W. van der Schee, “Heavy Ion Collisions: The Big Picture, and the Big Questions”, *Ann. Rev. Nucl. Part. Sci.* **68** (2018) 339–376, arXiv:1802.04801 [hep-ph].
- [2] J. Schukraft, “Ultra-relativistic heavy-ion collisions: Searching for the quark-gluon plasma”, *Nucl. Phys. A* **553** (1993) 31–44.
- [3] U. W. Heinz, “The Strongly coupled quark-gluon plasma created at RHIC”, *J. Phys. A* **42** (2009) 214003, arXiv:0810.5529 [nucl-th].

- [4] E. V. Shuryak, “Quantum Chromodynamics and the Theory of Superdense Matter”, *Phys. Rept.* **61** (1980) 71–158.
- [5] J. C. Collins and M. J. Perry, “Superdense Matter: Neutrons Or Asymptotically Free Quarks?”, *Phys. Rev. Lett.* **34** (1975) 1353.
- [6] ALICE Collaboration, “The ALICE experiment – A journey through QCD”, arXiv:2211.04384 [nucl-ex].
- [7] Y. Aoki, G. Endrodi, Z. Fodor, S. D. Katz, and K. K. Szabo, “The Order of the quantum chromodynamics transition predicted by the standard model of particle physics”, *Nature* **443** (2006) 675–678, arXiv:hep-lat/0611014.
- [8] F. R. Brown et al, “On the existence of a phase transition for QCD with three light quarks”, *Phys. Rev. Lett.* **65** (1990) 2491–2494.
- [9] A. Bzdak and V. Skokov, “Event-by-event fluctuations of magnetic and electric fields in heavy ion collisions”, *Phys. Lett.* **B710** (2012) 171–174, arXiv:1111.1949 [hep-ph].
- [10] T. D. Lee, “A Theory of Spontaneous T Violation”, *Phys. Rev. D* **8** (1973) 1226–1239.
- [11] T. D. Lee and G. C. Wick, “Vacuum Stability and Vacuum Excitation in a Spin 0 Field Theory”, *Phys. Rev.* **D9** (1974) 2291–2316.
- [12] D. Kharzeev, R. D. Pisarski, and M. H. G. Tytgat, “Possibility of spontaneous parity violation in hot QCD”, *Phys. Rev. Lett.* **81** (1998) 512–515, arXiv:hep-ph/9804221 [hep-ph].
- [13] P. D. Morley and I. A. Schmidt, “Strong P, CP, T Violations in Heavy Ion Collisions”, *Z. Phys.* **C26** (1985) 627.
- [14] D. Kharzeev and R. D. Pisarski, “Pionic measures of parity and CP violation in high-energy nuclear collisions”, *Phys. Rev.* **D61** (2000) 111901, arXiv:hep-ph/9906401 [hep-ph].
- [15] D. E. Kharzeev, “The Chiral Magnetic Effect and Anomaly-Induced Transport”, *Prog. Part. Nucl. Phys.* **75** (2014) 133–151, arXiv:1312.3348 [hep-ph].
- [16] D. E. Kharzeev, “Topology, magnetic field, and strongly interacting matter”, *Ann. Rev. Nucl. Part. Sci.* **65** (2015) 193–214, arXiv:1501.01336 [hep-ph].
- [17] D. E. Kharzeev and J. Liao, “Chiral magnetic effect reveals the topology of gauge fields in heavy-ion collisions”, *Nat Rev Phys* **3** (Jan., 2021) 55–63.
<http://www.nature.com/articles/s42254-020-00254-6>.
- [18] S. A. Voloshin, “Parity violation in hot QCD: How to detect it”, *Phys. Rev.* **C70** (2004) 057901, arXiv:hep-ph/0406311 [hep-ph].
- [19] D. Kharzeev and A. Zhitnitsky, “Charge separation induced by P-odd bubbles in QCD matter”, *Nucl. Phys.* **A797** (2007) 67–79, arXiv:0706.1026 [hep-ph].
- [20] K. Fukushima, D. E. Kharzeev, and H. J. Warringa, “The Chiral Magnetic Effect”, *Phys. Rev.* **D78** (2008) 074033, arXiv:0808.3382 [hep-ph].
- [21] D. E. Kharzeev, L. D. McLerran, and H. J. Warringa, “The Effects of topological charge change in heavy ion collisions: ’Event by event P and CP violation’”, *Nucl. Phys.* **A803** (2008) 227–253, arXiv:0711.0950 [hep-ph].

- [22] Q. Li et al, “Observation of the chiral magnetic effect in ZrTe5”, *Nature Phys.* **12** (2016) 550–554, arXiv:1412.6543 [cond-mat.str-el].
- [23] **STAR** Collaboration, B. I. Abelev et al., “Azimuthal Charged-Particle Correlations and Possible Local Strong Parity Violation”, *Phys. Rev. Lett.* **103** (2009) 251601, arXiv:0909.1739 [nucl-ex].
- [24] **STAR** Collaboration, B. I. Abelev et al., “Observation of charge-dependent azimuthal correlations and possible local strong parity violation in heavy ion collisions”, *Phys. Rev. C* **81** (2010) 054908, arXiv:0909.1717 [nucl-ex].
- [25] **ALICE** Collaboration, B. Abelev et al., “Charge separation relative to the reaction plane in Pb–Pb collisions at $\sqrt{s_{NN}} = 2.76$ TeV”, *Phys. Rev. Lett.* **110** (2013) 012301, arXiv:1207.0900 [nucl-ex].
- [26] S. Schlichting and S. Pratt, “Charge conservation at energies available at the BNL Relativistic Heavy Ion Collider and contributions to local parity violation observables”, *Phys. Rev.* **C83** (2011) 014913, arXiv:1009.4283 [nucl-th].
- [27] S. Pratt, S. Schlichting, and S. Gavin, “Effects of Momentum Conservation and Flow on Angular Correlations at RHIC”, *Phys. Rev.* **C84** (2011) 024909, arXiv:1011.6053 [nucl-th].
- [28] **STAR** Collaboration, L. Adamczyk et al., “Measurement of charge multiplicity asymmetry correlations in high-energy nucleus-nucleus collisions at $\sqrt{s_{NN}} = 200$ GeV”, *Phys. Rev.* **C89** (2014) 044908, arXiv:1303.0901 [nucl-ex].
- [29] **STAR** Collaboration, L. Adamczyk et al., “Fluctuations of charge separation perpendicular to the event plane and local parity violation in $\sqrt{s_{NN}} = 200$ GeV Au+Au collisions at the BNL Relativistic Heavy Ion Collider”, *Phys. Rev.* **C88** (2013) 064911, arXiv:1302.3802 [nucl-ex].
- [30] **STAR** Collaboration, L. Adamczyk et al., “Beam-energy dependence of charge separation along the magnetic field in Au+Au collisions at RHIC”, *Phys. Rev. Lett.* **113** (2014) 052302, arXiv:1404.1433 [nucl-ex].
- [31] **ALICE** Collaboration, S. Acharya et al., “Constraining the magnitude of the Chiral Magnetic Effect with Event Shape Engineering in Pb–Pb collisions at $\sqrt{s_{NN}} = 2.76$ TeV”, *Phys. Lett.* **B777** (2018) 151–162, arXiv:1709.04723 [nucl-ex].
- [32] **CMS** Collaboration, V. Khachatryan et al., “Observation of charge-dependent azimuthal correlations in p -Pb collisions and its implication for the search for the chiral magnetic effect”, *Phys. Rev. Lett.* **118** (2017) 122301, arXiv:1610.00263 [nucl-ex].
- [33] **STAR** Collaboration, J. Adam et al., “Charge-dependent pair correlations relative to a third particle in $p + Au$ and $d + Au$ collisions at RHIC”, *Phys. Lett.* **B798** (2019) 134975, arXiv:1906.03373 [nucl-ex].
- [34] **CMS** Collaboration, A. M. Sirunyan et al., “Constraints on the chiral magnetic effect using charge-dependent azimuthal correlations in pPb and $PbPb$ collisions at the CERN Large Hadron Collider”, *Phys. Rev.* **C97** (2018) 044912, arXiv:1708.01602 [nucl-ex].
- [35] J. Schukraft, A. Timmins, and S. A. Voloshin, “Ultra-relativistic nuclear collisions: event shape engineering”, *Phys. Lett.* **B719** (2013) 394–398, arXiv:1208.4563 [nucl-ex].
- [36] D. T. Son and A. R. Zhitnitsky, “Quantum anomalies in dense matter”, *Phys. Rev. D* **70** (2004) 074018, arXiv:hep-ph/0405216.

- [37] M. A. Metlitski and A. R. Zhitnitsky, “Anomalous axion interactions and topological currents in dense matter”, *Phys. Rev. D* **72** (2005) 045011, arXiv:hep-ph/0505072.
- [38] Y. Burnier, D. E. Kharzeev, J. Liao, and H.-U. Yee, “Chiral magnetic wave at finite baryon density and the electric quadrupole moment of quark-gluon plasma in heavy ion collisions”, *Phys. Rev. Lett.* **107** (2011) 052303, arXiv:1103.1307 [hep-ph].
- [39] Y. Burnier, D. E. Kharzeev, J. Liao, and H. U. Yee, “From the chiral magnetic wave to the charge dependence of elliptic flow”, arXiv:1208.2537 [hep-ph].
- [40] D. E. Kharzeev and H.-U. Yee, “Chiral Magnetic Wave”, *Phys. Rev. D* **83** (2011) 085007, arXiv:1012.6026 [hep-th].
- [41] H.-U. Yee and Y. Yin, “Realistic Implementation of Chiral Magnetic Wave in Heavy Ion Collisions”, *Phys. Rev. C* **89** (2014) 044909, arXiv:1311.2574 [nucl-th].
- [42] S. F. Taghavi and U. A. Wiedemann, “Chiral magnetic wave in an expanding QCD fluid”, *Phys. Rev. C* **91** (2015) 024902, arXiv:1310.0193 [hep-ph].
- [43] S. Voloshin and Y. Zhang, “Flow study in relativistic nuclear collisions by Fourier expansion of Azimuthal particle distributions”, *Z. Phys.* **C70** (1996) 665–672, arXiv:hep-ph/9407282 [hep-ph].
- [44] A. M. Poskanzer and S. A. Voloshin, “Methods for analyzing anisotropic flow in relativistic nuclear collisions”, *Phys. Rev.* **C58** (1998) 1671–1678, arXiv:nucl-ex/9805001 [nucl-ex].
- [45] **STAR** Collaboration, L. Adamczyk *et al.*, “Observation of charge asymmetry dependence of pion elliptic flow and the possible chiral magnetic wave in heavy-ion collisions”, *Phys. Rev. Lett.* **114** (2015) 252302, arXiv:1504.02175 [nucl-ex].
- [46] **ALICE** Collaboration, J. Adam *et al.*, “Charge-dependent flow and the search for the chiral magnetic wave in Pb–Pb collisions at $\sqrt{s_{NN}} = 2.76$ TeV”, *Phys. Rev. C* **93** (2016) 044903, arXiv:1512.05739 [nucl-ex].
- [47] W.-T. Deng and X.-G. Huang, “Event-by-event generation of electromagnetic fields in heavy-ion collisions”, *Phys. Rev. C* **85** (2012) 044907, arXiv:1201.5108 [nucl-th].
- [48] **CMS** Collaboration, A. M. Sirunyan *et al.*, “Probing the chiral magnetic wave in pPb and $PbPb$ collisions at $\sqrt{s_{NN}} = 5.02$ TeV using charge-dependent azimuthal anisotropies”, *Phys. Rev. C* **100** (2019) 064908, arXiv:1708.08901 [nucl-ex].
- [49] R. Belmont and J. L. Nagle, “To CME or not to CME? Implications of $p+Pb$ measurements of the chiral magnetic effect in heavy ion collisions”, *Phys. Rev. C* **96** (2017) 024901, arXiv:1610.07964 [nucl-th].
- [50] **STAR** Collaboration, M. I. Abdulhamid *et al.*, “Search for the chiral magnetic wave using anisotropic flow of identified particles at energies available at the BNL Relativistic Heavy Ion Collider”, *Phys. Rev. C* **108** (2023) 014908, arXiv:2210.14027 [nucl-ex].
- [51] C.-Z. Wang, W.-Y. Wu, Q.-Y. Shou, G.-L. Ma, Y.-G. Ma, and S. Zhang, “Interpreting the charge-dependent flow and constraining the chiral magnetic wave with event shape engineering”, *Phys. Lett. B* **820** (2021) 136580, arXiv:2104.05551 [nucl-th].
- [52] A. Bzdak and P. Bozek, “Contributions to the event-by-event charge asymmetry dependence for the elliptic flow of π^+ and π^- in heavy-ion collisions”, *Phys. Lett. B* **726** (2013) 239–243, arXiv:1303.1138 [nucl-th].

- [53] M. Stephanov and H.-U. Yee, “Charged elliptic flow at zero charge asymmetry”, *Phys. Rev. C* **88** (2013) 014908, arXiv:1304.6410 [nucl-th].
- [54] J. M. Campbell and M. A. Lisa, “Can baryon stopping explain the breakdown of constituent quark scaling and proposed signals of chiral magnetic waves at RHIC?”, *J. Phys. Conf. Ser.* **446** (2013) 012014.
- [55] S. A. Voloshin and R. Belmont, “Measuring and interpreting charge dependent anisotropic flow”, *Nucl. Phys. A* **931** (2014) 992–996, arXiv:1408.0714 [nucl-ex].
- [56] Y. Hatta, A. Monnai, and B.-W. Xiao, “Elliptic flow difference of charged pions in heavy-ion collisions”, *Nucl. Phys. A* **947** (2016) 155–160, arXiv:1507.04690 [hep-ph].
- [57] M. Hongo, Y. Hirono, and T. Hirano, “Anomalous-hydrodynamic analysis of charge-dependent elliptic flow in heavy-ion collisions”, *Phys. Lett. B* **775** (2017) 266–270, arXiv:1309.2823 [nucl-th].
- [58] X.-L. Zhao, G.-L. Ma, and Y.-G. Ma, “Novel mechanism for electric quadrupole moment generation in relativistic heavy-ion collisions”, *Phys. Lett. B* **792** (2019) 413–418, arXiv:1901.04156 [hep-ph].
- [59] H.-j. Xu, J. Zhao, Y. Feng, and F. Wang, “Complications in the interpretation of the charge asymmetry dependent π flow for the chiral magnetic wave”, *Phys. Rev. C* **101** (2020) 014913, arXiv:1910.02896 [nucl-th].
- [60] S. A. Bass, P. Danielewicz, and S. Pratt, “Clocking hadronization in relativistic heavy ion collisions with balance functions”, *Phys. Rev. Lett.* **85** (2000) 2689–2692, arXiv:nucl-th/0005044.
- [61] ALICE Collaboration, B. Abelev *et al.*, “Charge correlations using the balance function in Pb–Pb collisions at $\sqrt{s_{NN}} = 2.76$ TeV”, *Phys. Lett. B* **723** (2013) 267–279, arXiv:1301.3756 [nucl-ex].
- [62] W.-Y. Wu, C.-Z. Wang, Q.-Y. Shou, Y.-G. Ma, and L. Zheng, “Charge-dependent transverse momentum and its impact on the search for the chiral magnetic wave”, *Phys. Rev. C* **103** (2021) 034906, arXiv:2010.09955 [nucl-th].
- [63] G.-L. Ma, “Final state effects on charge asymmetry of pion elliptic flow in high-energy heavy-ion collisions”, *Phys. Lett. B* **735** (2014) 383–386, arXiv:1401.6502 [nucl-th].
- [64] W.-H. Zhou and J. Xu, “Simulating the Chiral Magnetic Wave in a Box System”, *Phys. Rev. C* **98** (2018) 044904, arXiv:1810.01030 [nucl-th].
- [65] Z.-Z. Han and J. Xu, “Charge asymmetry dependence of the elliptic flow splitting in relativistic heavy-ion collisions”, *Phys. Rev. C* **99** (2019) 044915, arXiv:1904.03544 [nucl-th].
- [66] D. Shen, J. Chen, G. Ma, Y.-G. Ma, Q. Shou, S. Zhang, and C. Zhong, “Charge asymmetry dependence of flow and a novel correlator to detect the chiral magnetic wave in a multiphase transport model”, *Phys. Rev. C* **100** (2019) 064907, arXiv:1911.00839 [hep-ph].
- [67] N. Magdy, M.-W. Nie, L. Huang, G.-L. Ma, and R. A. Lacey, “An extended $R_{\Psi_m}^{(2)}(\Delta S_2)$ correlator for detecting and characterizing the Chiral Magnetic Wave”, *Phys. Lett. B* **811** (2020) 135986, arXiv:2003.02396 [nucl-ex].

- [68] S. Shi, Y. Jiang, E. Lilleskov, and J. Liao, “Anomalous Chiral Transport in Heavy Ion Collisions from Anomalous-Viscous Fluid Dynamics”, *Annals Phys.* **394** (2018) 50–72, arXiv:1711.02496 [nucl-th].
- [69] W.-Y. Wu *et al.*, “Global constraint on the magnitude of anomalous chiral effects in heavy-ion collisions”, *Phys. Rev. C* **107** (2023) L031902, arXiv:2211.15446 [nucl-th].
- [70] ALICE Collaboration, K. Aamodt *et al.*, “The ALICE experiment at the CERN LHC”, *JINST* **3** (2008) S08002.
- [71] ALICE Collaboration, B. B. Abelev *et al.*, “Performance of the ALICE Experiment at the CERN LHC”, *Int. J. Mod. Phys. A* **29** (2014) 1430044, arXiv:1402.4476 [nucl-ex].
- [72] J. Alme *et al.*, “The ALICE TPC, a large 3-dimensional tracking device with fast readout for ultra-high multiplicity events”, *Nucl. Instrum. Meth. A* **622** (2010) 316–367, arXiv:1001.1950 [physics.ins-det].
- [73] ALICE Collaboration, G. Dellacasa *et al.*, “ALICE technical design report of the time-of-flight system (TOF)”, *CERN-LHCC-2000-012*.
- [74] ALICE Collaboration, E. Abbas *et al.*, “Performance of the ALICE VZERO system”, *JINST* **8** (2013) P10016, arXiv:1306.3130 [nucl-ex].
- [75] ALICE Collaboration, S. Acharya *et al.*, “Constraining the Chiral Magnetic Effect with charge-dependent azimuthal correlations in Pb–Pb collisions at $\sqrt{s_{NN}} = 2.76$ and 5.02 TeV”, *JHEP* **09** (2020) 160, arXiv:2005.14640 [nucl-ex].
- [76] ALICE Collaboration, B. Abelev *et al.*, “Centrality determination of Pb–Pb collisions at $\sqrt{s_{NN}} = 2.76$ TeV with ALICE”, *Phys. Rev. C* **88** (2013) 044909, arXiv:1301.4361 [nucl-ex].
- [77] M. Gyulassy and X.-N. Wang, “HIJING 1.0: A Monte Carlo program for parton and particle production in high-energy hadronic and nuclear collisions”, *Comput. Phys. Commun.* **83** (1994) 307, arXiv:nucl-th/9502021.
- [78] R. Brun, F. Bruyant, F. Carminati, S. Giani, M. Maire, A. McPherson, G. Patrick, and L. Urban, “GEANT Detector Description and Simulation Tool”, *CERN Program Library, CERN, Geneva* (1993).
- [79] A. Bilandzic, R. Snellings, and S. Voloshin, “Flow analysis with cumulants: Direct calculations”, *Phys. Rev. C* **83** (2011) 044913, arXiv:1010.0233 [nucl-ex].
- [80] Y. Zhou, X. Zhu, P. Li, and H. Song, “Investigation of possible hadronic flow in $\sqrt{s_{NN}} = 5.02$ TeV $p - Pb$ collisions”, *Phys. Rev. C* **91** (2015) 064908, arXiv:1503.06986 [nucl-th].
- [81] R. Barlow, “Systematic errors: Facts and fictions”, in *Advanced Statistical Techniques in Particle Physics. Proceedings, Conference, Durham, UK, March 18-22, 2002*, pp. 134–144. 2002. arXiv:hep-ex/0207026 [hep-ex].
- [82] H.-j. Xu, J. Zhao, Y. Feng, and F. Wang, “Importance of non-flow background on the chiral magnetic wave search”, *Nucl. Phys. A* **1005** (2021) 121770, arXiv:2002.05220 [nucl-th].
- [83] ALICE Collaboration, J. Adam *et al.*, “Correlated event-by-event fluctuations of flow harmonics in Pb–Pb collisions at $\sqrt{s_{NN}} = 2.76$ TeV”, *Phys. Rev. Lett.* **117** (2016) 182301, arXiv:1604.07663 [nucl-ex].














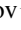




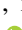
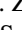
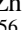




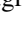

- [84] **ALICE** Collaboration, K. Aamodt *et al.*, “Higher harmonic anisotropic flow measurements of charged particles in Pb–Pb collisions at $\sqrt{s_{NN}}=2.76$ TeV”, *Phys. Rev. Lett.* **107** (2011) 032301, arXiv:1105.3865 [nucl-ex].
- [85] **ATLAS** Collaboration, G. Aad *et al.*, “Measurement of event-plane correlations in $\sqrt{s_{NN}} = 2.76$ TeV lead-lead collisions with the ATLAS detector”, *Phys. Rev. C* **90** (2014) 024905, arXiv:1403.0489 [hep-ex].
- [86] Y. Hatta, “Analytic approaches to relativistic hydrodynamics”, *Nucl. Phys. A* **956** (2016) 152–159, arXiv:1601.04128 [hep-ph].

A The ALICE Collaboration

S. Acharya ¹²⁶, D. Adamová ⁸⁶, G. Aglieri Rinella ³³, M. Agnello ³⁰, N. Agrawal ⁵¹, Z. Ahammed ¹³⁴, S. Ahmad ¹⁶, S.U. Ahn ⁷¹, I. Ahuja ³⁸, A. Akhmedov ¹⁴², M. Al-Turany ⁹⁷, D. Aleksandrov ¹⁴², B. Alessandro ⁵⁶, H.M. Alfandi ⁶, R. Alfaro Molina ⁶⁷, B. Ali ¹⁶, A. Alici ²⁶, N. Alizadehvandchali ¹¹⁵, A. Alkin ³³, J. Alme ²¹, G. Alocco ⁵², T. Alt ⁶⁴, A.R. Altamura ⁵⁰, I. Altsybeev ⁹⁵, M.N. Anaam ⁶, C. Andrei ⁴⁶, N. Andreou ¹¹⁴, A. Andronic ¹³⁷, V. Anguelov ⁹⁴, F. Antinori ⁵⁴, P. Antonioli ⁵¹, N. Apadula ⁷⁴, L. Aphecetche ¹⁰³, H. Appelshäuser ⁶⁴, C. Arata ⁷³, S. Arcelli ²⁶, M. Aresti ²³, R. Arnaldi ⁵⁶, J.G.M.C.A. Arneiro ¹¹⁰, I.C. Arsene ²⁰, M. Arslanod ¹³⁹, A. Augustinus ³³, R. Averbeck ⁹⁷, M.D. Azmi ¹⁶, H. Baba ¹²³, A. Badalà ⁵³, J. Bae ¹⁰⁴, Y.W. Baek ⁴¹, X. Bai ¹¹⁹, R. Bailhache ⁶⁴, Y. Bailung ⁴⁸, A. Balbino ³⁰, A. Baldisseri ¹²⁹, B. Balis ², D. Banerjee ⁴, Z. Banoo ⁹¹, R. Barbera ²⁷, F. Barile ³², L. Barioglio ⁹⁵, M. Barlou ⁷⁸, B. Barman ⁴², G.G. Barnaföldi ¹³⁸, L.S. Barnby ⁸⁵, V. Barret ¹²⁶, L. Barreto ¹¹⁰, C. Bartels ¹¹⁸, K. Barth ³³, E. Bartsch ⁶⁴, N. Bastid ¹²⁶, S. Basu ⁷⁵, G. Batigne ¹⁰³, D. Battistini ⁹⁵, B. Batyunya ¹⁴³, D. Bauri ⁴⁷, J.L. Bazo Alba ¹⁰¹, I.G. Bearden ⁸³, C. Beattie ¹³⁹, P. Becht ⁹⁷, D. Behera ⁴⁸, I. Belikov ¹²⁸, A.D.C. Bell Hechavarria ¹³⁷, F. Bellini ²⁶, R. Bellwied ¹¹⁵, S. Belokurova ¹⁴², Y.A.V. Beltran ⁴⁵, G. Bencedi ¹³⁸, S. Beole ²⁵, Y. Berdnikov ¹⁴², A. Berdnikova ⁹⁴, L. Bergmann ⁹⁴, M.G. Besoiu ⁶³, L. Betev ³³, P.P. Bhaduri ¹³⁴, A. Bhasin ⁹¹, M.A. Bhat ⁴, B. Bhattacharjee ⁴², L. Bianchi ²⁵, N. Bianchi ⁴⁹, J. Bielčík ³⁶, J. Bielčíková ⁸⁶, J. Biernat ¹⁰⁷, A.P. Bigot ¹²⁸, A. Bilandzic ⁹⁵, G. Biro ¹³⁸, S. Biswas ⁴, N. Bize ¹⁰³, J.T. Blair ¹⁰⁸, D. Blau ¹⁴², M.B. Blidaru ⁹⁷, N. Bluhme ³⁹, C. Blume ⁶⁴, G. Boca ^{22,55}, F. Bock ⁸⁷, T. Bodova ²¹, A. Bogdanov ¹⁴², S. Boi ²³, J. Bok ⁵⁸, L. Boldizsár ¹³⁸, M. Bombara ³⁸, P.M. Bond ³³, G. Bonomi ^{133,55}, H. Borel ¹²⁹, A. Borissov ¹⁴², A.G. Borquez Carcamo ⁹⁴, H. Bossi ¹³⁹, E. Botta ²⁵, Y.E.M. Bouziani ⁶⁴, L. Bratrud ⁶⁴, P. Braun-Munzinger ⁹⁷, M. Bregant ¹¹⁰, M. Broz ³⁶, G.E. Bruno ^{96,32}, M.D. Buckland ²⁴, D. Budnikov ¹⁴², H. Buesching ⁶⁴, S. Bufalino ³⁰, P. Buhler ¹⁰², N. Burmasov ¹⁴², Z. Buthelezi ^{68,122}, A. Bylinkin ²¹, S.A. Bysiak ¹⁰⁷, M. Cai ⁶, H. Caines ¹³⁹, A. Caliva ²⁹, E. Calvo Villar ¹⁰¹, J.M.M. Camacho ¹⁰⁹, P. Camerini ²⁴, F.D.M. Canedo ¹¹⁰, M. Carabas ¹²⁵, A.A. Carballo ³³, F. Carnesecchi ³³, R. Caron ¹²⁷, L.A.D. Carvalho ¹¹⁰, J. Castillo Castellanos ¹²⁹, F. Catalano ^{33,25}, C. Ceballos Sanchez ¹⁴³, I. Chakaberia ⁷⁴, P. Chakraborty ⁴⁷, S. Chandra ¹³⁴, S. Chapeland ³³, M. Chartier ¹¹⁸, S. Chattopadhyay ¹³⁴, S. Chattopadhyay ⁹⁹, T.G. Chavez ⁴⁵, T. Cheng ^{97,6}, C. Cheshkov ¹²⁷, B. Cheynis ¹²⁷, V. Chibante Barroso ³³, D.D. Chinellato ¹¹¹, E.S. Chizzali ^{1,95}, J. Cho ⁵⁸, S. Cho ⁵⁸, P. Chochula ³³, D. Choudhury ⁴², P. Christakoglou ⁸⁴, C.H. Christensen ⁸³, P. Christiansen ⁷⁵, T. Chujo ¹²⁴, M. Ciacco ³⁰, C. Cicalo ⁵², F. Cindolo ⁵¹, M.R. Ciupek ⁹⁷, G. Clai ^{II,51}, F. Colamaria ⁵⁰, J.S. Colburn ¹⁰⁰, D. Colella ^{96,32}, M. Colocci ²⁶, M. Concas ^{III,33}, G. Conesa Balbastre ⁷³, Z. Conesa del Valle ¹³⁰, G. Contin ²⁴, J.G. Contreras ³⁶, M.L. Coquet ¹²⁹, P. Cortese ^{132,56}, M.R. Cosentino ¹¹², F. Costa ³³, S. Costanza ^{22,55}, C. Cot ¹³⁰, J. Crkovská ⁹⁴, P. Crochet ¹²⁶, R. Cruz-Torres ⁷⁴, P. Cui ⁶, A. Dainese ⁵⁴, M.C. Danisch ⁹⁴, A. Danu ⁶³, P. Das ⁸⁰, P. Das ⁴, S. Das ⁴, A.R. Dash ¹³⁷, S. Dash ⁴⁷, R.M.H. David ⁴⁵, A. De Caro ²⁹, G. de Cataldo ⁵⁰, J. de Cuveland ³⁹, A. De Falco ²³, D. De Gruttola ²⁹, N. De Marco ⁵⁶, C. De Martin ²⁴, S. De Pasquale ²⁹, R. Deb ¹³³, R. Del Grande ⁹⁵, L. Dello Stritto ²⁹, W. Deng ⁶, P. Dhankher ¹⁹, D. Di Bari ³², A. Di Mauro ³³, B. Diab ¹²⁹, R.A. Diaz ^{143,7}, T. Dietel ¹¹³, Y. Ding ⁶, J. Ditzel ⁶⁴, R. Divià ³³, D.U. Dixit ¹⁹, Ø. Djuvsland ²¹, U. Dmitrieva ¹⁴², A. Dobrin ⁶³, B. Dönigus ⁶⁴, J.M. Dubinski ¹³⁵, A. Dubla ⁹⁷, S. Dudi ⁹⁰, P. Dupieux ¹²⁶, M. Durkac ¹⁰⁶, N. Dzalaiova ¹³, T.M. Eder ¹³⁷, R.J. Ehlers ⁷⁴, F. Eisenhut ⁶⁴, R. Ejima ⁹², D. Elia ⁵⁰, B. Erazmus ¹⁰³, F. Ercolessi ²⁶, B. Espagnon ¹³⁰, G. Eulisse ³³, D. Evans ¹⁰⁰, S. Evdokimov ¹⁴², L. Fabbietti ⁹⁵, M. Faggin ²⁸, J. Faivre ⁷³, F. Fan ⁶, W. Fan ⁷⁴, A. Fantoni ⁴⁹, M. Fasel ⁸⁷, A. Feliciello ⁵⁶, G. Feofilov ¹⁴², A. Fernández Téllez ⁴⁵, L. Ferrandi ¹¹⁰, M.B. Ferrer ³³, A. Ferrero ¹²⁹, C. Ferrero ⁵⁶, A. Ferretti ²⁵, V.J.G. Feuillard ⁹⁴, V. Filova ³⁶, D. Finogeev ¹⁴², F.M. Fionda ⁵², E. Flatland ³³, F. Flor ¹¹⁵, A.N. Flores ¹⁰⁸, S. Foertsch ⁶⁸, I. Fokin ⁹⁴, S. Fokin ¹⁴², E. Fragiaco ⁵⁷, E. Frajna ¹³⁸, U. Fuchs ³³, N. Funicello ²⁹, C. Furget ⁷³, A. Furs ¹⁴², T. Fusayasu ⁹⁸, J.J. Gaardhøje ⁸³, M. Gagliardi ²⁵, A.M. Gago ¹⁰¹, T. Gahlaut ⁴⁷, C.D. Galvan ¹⁰⁹, D.R. Gangadharan ¹¹⁵, P. Ganoti ⁷⁸, C. Garabatos ⁹⁷, A.T. Garcia ¹³⁰, J.R.A. Garcia ⁴⁵, E. Garcia-Solis ⁹, C. Gargiulo ³³, P. Gasik ⁹⁷, A. Gautam ¹¹⁷, M.B. Gay Ducati ⁶⁶, M. Germain ¹⁰³, A. Ghimouz ¹²⁴, C. Ghosh ¹³⁴, M. Giacalone ⁵¹, G. Gioachin ³⁰, P. Giubellino ^{97,56}, P. Giubilato ²⁸, A.M.C. Glaenger ¹²⁹, P. Glässel ⁹⁴, E. Glimos ¹²¹, D.J.Q. Goh ⁷⁶, V. Gonzalez ¹³⁶, P. Gordeev ¹⁴², M. Gorgon ², K. Goswami ⁴⁸, S. Gotovac ³⁴, V. Grabski ⁶⁷, L.K. Graczykowski ¹³⁵, E. Grecka ⁸⁶, A. Grelli ⁵⁹, C. Grigoras ³³, V. Grigoriev ¹⁴², S. Grigoryan ^{143,1}, F. Grosa ³³, J.F. Grosse-Oetringhaus ³³, R. Grosso ⁹⁷, D. Grund ³⁶, N.A. Grunwald ⁹⁴, G.G. Guardiano ¹¹¹, R. Guernane ⁷³, M. Guilbaud ¹⁰³, K. Gulbrandsen ⁸³, T. Gündem ⁶⁴, T. Gunji ¹²³,

W. Guo ⁶, A. Gupta ⁹¹, R. Gupta ⁹¹, R. Gupta ⁴⁸, S.P. Guzman ⁴⁵, K. Gwizdziel ¹³⁵, L. Gyulai ¹³⁸, C. Hadjidakis ¹³⁰, F.U. Haider ⁹¹, S. Haidlova ³⁶, H. Hamagaki ⁷⁶, A. Hamdi ⁷⁴, Y. Han ¹⁴⁰, B.G. Hanley ¹³⁶, R. Hannigan ¹⁰⁸, J. Hansen ⁷⁵, M.R. Haque ¹³⁵, J.W. Harris ¹³⁹, A. Harton ⁹, H. Hassan ¹¹⁶, D. Hatzifotiadou ⁵¹, P. Hauer ⁴³, L.B. Havener ¹³⁹, S.T. Heckel ⁹⁵, E. Hellbär ⁹⁷, H. Helstrup ³⁵, M. Hemmer ⁶⁴, T. Herman ³⁶, G. Herrera Corral ⁸, F. Herrmann ¹³⁷, S. Herrmann ¹²⁷, K.F. Hetland ³⁵, B. Heybeck ⁶⁴, H. Hillemanns ³³, B. Hippolyte ¹²⁸, F.W. Hoffmann ⁷⁰, B. Hofman ⁵⁹, G.H. Hong ¹⁴⁰, M. Horst ⁹⁵, A. Horzyk ², Y. Hou ⁶, P. Hristov ³³, C. Hughes ¹²¹, P. Huhn ⁶⁴, L.M. Huhta ¹¹⁶, T.J. Humanic ⁸⁸, A. Hutson ¹¹⁵, D. Hutter ³⁹, R. Ilkaev ¹⁴², H. Ilyas ¹⁴, M. Inaba ¹²⁴, G.M. Innocenti ³³, M. Ippolitov ¹⁴², A. Isakov ^{84,86}, T. Isidori ¹¹⁷, M.S. Islam ⁹⁹, M. Ivanov ⁹⁷, M. Ivanov ¹³, V. Ivanov ¹⁴², K.E. Iversen ⁷⁵, M. Jablonski ², B. Jacak ⁷⁴, N. Jacazio ²⁶, P.M. Jacobs ⁷⁴, S. Jadlovská ¹⁰⁶, J. Jadlovsky ¹⁰⁶, S. Jaelani ⁸², C. Jahnke ¹¹⁰, M.J. Jakubowska ¹³⁵, M.A. Janik ¹³⁵, T. Janson ⁷⁰, S. Ji ¹⁷, S. Jia ¹⁰, A.A.P. Jimenez ⁶⁵, F. Jonas ⁸⁷, D.M. Jones ¹¹⁸, J.M. Jowett ^{33,97}, J. Jung ⁶⁴, M. Jung ⁶⁴, A. Junique ³³, A. Jusko ¹⁰⁰, M.J. Kabus ^{33,135}, J. Kaewjai ¹⁰⁵, P. Kalinak ⁶⁰, A.S. Kalteyer ⁹⁷, A. Kalweit ³³, V. Kaplin ¹⁴², A. Karasu Uysal ⁷², D. Karatovic ⁸⁹, O. Karavichev ¹⁴², T. Karavicheva ¹⁴², P. Karczmarczyk ¹³⁵, E. Karpechev ¹⁴², U. Kebschull ⁷⁰, R. Keidel ¹⁴¹, D.L.D. Keijndener ⁵⁹, M. Keil ³³, B. Ketzer ⁴³, S.S. Khade ⁴⁸, A.M. Khan ¹¹⁹, S. Khan ¹⁶, A. Khanzadeev ¹⁴², Y. Kharlov ¹⁴², A. Khatun ¹¹⁷, A. Khuntia ³⁶, B. Kileng ³⁵, B. Kim ¹⁰⁴, C. Kim ¹⁷, D.J. Kim ¹¹⁶, E.J. Kim ⁶⁹, J. Kim ¹⁴⁰, J.S. Kim ⁴¹, J. Kim ⁵⁸, J. Kim ⁶⁹, M. Kim ¹⁹, S. Kim ¹⁸, T. Kim ¹⁴⁰, K. Kimura ⁹², S. Kirsch ⁶⁴, I. Kisel ³⁹, S. Kiselev ¹⁴², A. Kisiel ¹³⁵, J.P. Kitowski ², J.L. Klay ⁵, J. Klein ³³, S. Klein ⁷⁴, C. Klein-Bösing ¹³⁷, M. Kleiner ⁶⁴, T. Klemenz ⁹⁵, A. Kluge ³³, A.G. Knospe ¹¹⁵, C. Kobdaj ¹⁰⁵, T. Kollegger ⁹⁷, A. Kondratyev ¹⁴³, N. Kondratyeva ¹⁴², E. Kondratyuk ¹⁴², J. König ⁶⁴, S.A. Königstorfer ⁹⁵, P.J. Konopka ³³, G. Kornakov ¹³⁵, S.D. Koryciak ², A. Kotliarov ⁸⁶, V. Kovalenko ¹⁴², M. Kowalski ¹⁰⁷, V. Kozuharov ³⁷, I. Králik ⁶⁰, A. Kravčáková ³⁸, L. Krcal ^{33,39}, M. Krivda ^{100,60}, F. Krizek ⁸⁶, K. Krizkova Gajdosova ³³, M. Kroesen ⁹⁴, M. Krüger ⁶⁴, D.M. Krupova ³⁶, E. Kryshen ¹⁴², V. Kučera ⁵⁸, C. Kuhn ¹²⁸, P.G. Kuijer ⁸⁴, T. Kumaoka ¹²⁴, D. Kumar ¹³⁴, L. Kumar ⁹⁰, N. Kumar ⁹⁰, S. Kumar ³², S. Kundu ³³, P. Kurashvili ⁷⁹, A. Kurepin ¹⁴², A.B. Kurepin ¹⁴², A. Kuryakin ¹⁴², S. Kushpil ⁸⁶, V. Kuskov ¹⁴², M.J. Kweon ⁵⁸, Y. Kwon ¹⁴⁰, S.L. La Pointe ³⁹, P. La Rocca ²⁷, A. Lakrathok ¹⁰⁵, M. Lamanna ³³, R. Langoy ¹²⁰, P. Larionov ³³, E. Laudi ³³, L. Lautner ^{33,95}, R. Lavicka ¹⁰², R. Lea ^{133,55}, H. Lee ¹⁰⁴, I. Legrand ⁴⁶, G. Legras ¹³⁷, J. Lehrbach ³⁹, T.M. Lelek ², R.C. Lemmon ⁸⁵, I. León Monzón ¹⁰⁹, M.M. Lesch ⁹⁵, E.D. Lesser ¹⁹, P. Lévai ¹³⁸, X. Li ¹⁰, J. Lien ¹²⁰, R. Lietava ¹⁰⁰, I. Likmeta ¹¹⁵, B. Lim ²⁵, S.H. Lim ¹⁷, V. Lindenstruth ³⁹, A. Lindner ⁴⁶, C. Lippmann ⁹⁷, D.H. Liu ⁶, J. Liu ¹¹⁸, G.S.S. Liveraro ¹¹¹, I.M. Lofnes ²¹, C. Loizides ⁸⁷, S. Lokos ¹⁰⁷, J. Lomker ⁵⁹, P. Loncar ³⁴, X. Lopez ¹²⁶, E. López Torres ⁷, P. Lu ^{97,119}, F.V. Lugo ⁶⁷, J.R. Luhder ¹³⁷, M. Lunardon ²⁸, G. Luparello ⁵⁷, Y.G. Ma ⁴⁰, M. Mager ³³, A. Maire ¹²⁸, M.V. Makariev ³⁷, M. Malaev ¹⁴², G. Malfattore ²⁶, N.M. Malik ⁹¹, Q.W. Malik ²⁰, S.K. Malik ⁹¹, L. Malinina ^{VI,143}, D. Mallick ^{130,80}, N. Mallick ⁴⁸, G. Mandaglio ^{31,53}, S.K. Mandal ⁷⁹, V. Manko ¹⁴², F. Manso ¹²⁶, V. Manzari ⁵⁰, Y. Mao ⁶, R.W. Marcjan ², G.V. Margagliotti ²⁴, A. Margotti ⁵¹, A. Marín ⁹⁷, C. Markert ¹⁰⁸, P. Martinengo ³³, M.I. Martínez ⁴⁵, G. Martínez García ¹⁰³, M.P.P. Martins ¹¹⁰, S. Masciocchi ⁹⁷, M. Masera ²⁵, A. Masoni ⁵², L. Massacrier ¹³⁰, O. Massen ⁵⁹, A. Mastroserio ^{131,50}, O. Matonoha ⁷⁵, S. Mattiazzo ²⁸, A. Matyja ¹⁰⁷, C. Mayer ¹⁰⁷, A.L. Mazuecos ³³, F. Mazzaschi ²⁵, M. Mazzilli ³³, J.E. Mdhuli ¹²², Y. Melikyan ⁴⁴, A. Menchaca-Rocha ⁶⁷, J.E.M. Mendez ⁶⁵, E. Meninno ^{102,29}, A.S. Menon ¹¹⁵, M. Meres ¹³, S. Mhlanga ^{113,68}, Y. Miake ¹²⁴, L. Micheletti ³³, D.L. Mihaylov ⁹⁵, K. Mikhaylov ^{143,142}, A.N. Mishra ¹³⁸, D. Miśkowiec ⁹⁷, A. Modak ⁴, B. Mohanty ⁸⁰, M. Mohisin Khan ^{IV,16}, M.A. Molander ⁴⁴, S. Monira ¹³⁵, C. Mordasini ¹¹⁶, D.A. Moreira De Godoy ¹³⁷, I. Morozov ¹⁴², A. Morsch ³³, T. Mrnjavac ³³, V. Muccifora ⁴⁹, S. Muhuri ¹³⁴, J.D. Mulligan ⁷⁴, A. Mulliri ²³, M.G. Munhoz ¹¹⁰, R.H. Munzer ⁶⁴, H. Murakami ¹²³, S. Murray ¹¹³, L. Musa ³³, J. Musinsky ⁶⁰, J.W. Myrcha ¹³⁵, B. Naik ¹²², A.I. Nambrath ¹⁹, B.K. Nandi ⁴⁷, R. Nania ⁵¹, E. Nappi ⁵⁰, A.F. Nassirpour ¹⁸, A. Nath ⁹⁴, C. Natrass ¹²¹, M.N. Naydenov ³⁷, A. Neagu ²⁰, A. Negru ¹²⁵, E. Nekrasova ¹⁴², L. Nellen ⁶⁵, R. Nepeivoda ⁷⁵, S. Nese ²⁰, G. Neskovic ³⁹, N. Nicassio ⁵⁰, B.S. Nielsen ⁸³, E.G. Nielsen ⁸³, S. Nikolaev ¹⁴², S. Nikulin ¹⁴², V. Nikulin ¹⁴², F. Noferini ⁵¹, S. Noh ¹², P. Nomokonov ¹⁴³, J. Norman ¹¹⁸, N. Novitzky ⁸⁷, P. Nowakowski ¹³⁵, A. Nyanin ¹⁴², J. Nystrand ²¹, M. Ogino ⁷⁶, S. Oh ¹⁸, A. Ohlson ⁷⁵, V.A. Okorokov ¹⁴², J. Oleniacz ¹³⁵, A.C. Oliveira Da Silva ¹²¹, A. Onnerstad ¹¹⁶, C. Oppedisano ⁵⁶, A. Ortiz Velasquez ⁶⁵, J. Otwinowski ¹⁰⁷, M. Oya ⁹², K. Oyama ⁷⁶, Y. Pachmayer ⁹⁴, S. Padhan ⁴⁷, D. Pagano ^{133,55}, G. Paic ⁶⁵, A. Palasciano ⁵⁰, S. Panebianco ¹²⁹,

H. Park ¹²⁴, H. Park ¹⁰⁴, J. Park ⁵⁸, J.E. Parkkila ³³, Y. Patley ⁴⁷, R.N. Patra⁹¹, B. Paul ²³, H. Pei ⁶, T. Peitzmann ⁵⁹, X. Peng ¹¹, M. Pennisi ²⁵, S. Perciballi ²⁵, D. Peresunko ¹⁴², G.M. Perez ⁷, Y. Pestov¹⁴², V. Petrov ¹⁴², M. Petrovici ⁴⁶, R.P. Pezzi ^{103,66}, S. Piano ⁵⁷, M. Pikna ¹³, P. Pillot ¹⁰³, O. Pinazza ^{51,33}, L. Pinsky¹¹⁵, C. Pinto ⁹⁵, S. Pisano ⁴⁹, M. Płoskoń ⁷⁴, M. Planinic⁸⁹, F. Pliquett⁶⁴, M.G. Poghosyan ⁸⁷, B. Polichtchouk ¹⁴², S. Politano ³⁰, N. Poljak ⁸⁹, A. Pop ⁴⁶, S. Porteboeuf-Houssais ¹²⁶, V. Pozdniakov ¹⁴³, I.Y. Pozos ⁴⁵, K.K. Pradhan ⁴⁸, S.K. Prasad ⁴, S. Prasad ⁴⁸, R. Preghenella ⁵¹, F. Prino ⁵⁶, C.A. Pruneau ¹³⁶, I. Pshenichnov ¹⁴², M. Puccio ³³, S. Pucillo ²⁵, Z. Pugelova¹⁰⁶, S. Qiu ⁸⁴, L. Quaglia ²⁵, S. Ragoni ¹⁵, A. Rai ¹³⁹, A. Rakotozafindrabe ¹²⁹, L. Ramello ^{132,56}, F. Rami ¹²⁸, S.A.R. Ramirez ⁴⁵, T.A. Rancien⁷³, M. Rasa ²⁷, S.S. Räsänen ⁴⁴, R. Rath ⁵¹, M.P. Rauch ²¹, I. Ravasenga ⁸⁴, K.F. Read ^{87,121}, C. Reckziegel ¹¹², A.R. Redelbach ³⁹, K. Redlich ^{V,79}, C.A. Reetz ⁹⁷, A. Rehman²¹, F. Reidt ³³, H.A. Reme-Ness ³⁵, Z. Rescakova³⁸, K. Reygers ⁹⁴, A. Riabov ¹⁴², V. Riabov ¹⁴², R. Ricci ²⁹, M. Richter ²⁰, A.A. Riedel ⁹⁵, W. Riegler ³³, A.G. Riffero ²⁵, C. Ristea ⁶³, M.V. Rodriguez ³³, M. Rodríguez Cahuantzi ⁴⁵, K. Røed ²⁰, R. Rogalev ¹⁴², E. Rogochaya ¹⁴³, T.S. Rogoschinski ⁶⁴, D. Rohr ³³, D. Röhrich ²¹, P.F. Rojas⁴⁵, S. Rojas Torres ³⁶, P.S. Rokita ¹³⁵, G. Romanenko ²⁶, F. Ronchetti ⁴⁹, A. Rosano ^{31,53}, E.D. Rosas⁶⁵, K. Roslon ¹³⁵, A. Rossi ⁵⁴, A. Roy ⁴⁸, S. Roy ⁴⁷, N. Rubini ²⁶, D. Ruggiano ¹³⁵, R. Rui ²⁴, P.G. Russek ², R. Russo ⁸⁴, A. Rustamov ⁸¹, E. Ryabinkin ¹⁴², Y. Ryabov ¹⁴², A. Rybicki ¹⁰⁷, H. Rytkonen ¹¹⁶, J. Ryu ¹⁷, W. Rzesza ¹³⁵, O.A.M. Saariimaki ⁴⁴, S. Sadhu ³², S. Sadovsky ¹⁴², J. Saetre ²¹, K. Šafařík ³⁶, P. Saha⁴², S.K. Saha ⁴, S. Saha ⁸⁰, B. Sahoo ⁴⁷, B. Sahoo ⁴⁸, R. Sahoo ⁴⁸, S. Sahoo⁶¹, D. Sahu ⁴⁸, P.K. Sahu ⁶¹, J. Saini ¹³⁴, K. Sajdakova³⁸, S. Sakai ¹²⁴, M.P. Salvan ⁹⁷, S. Sambyal ⁹¹, D. Samitz ¹⁰², I. Sanna ^{33,95}, T.B. Saramela¹¹⁰, P. Sarma ⁴², V. Sarritzu ²³, V.M. Sarti ⁹⁵, M.H.P. Sas ³³, S. Sawan⁸⁰, J. Schambach ⁸⁷, H.S. Scheid ⁶⁴, C. Schiaua ⁴⁶, R. Schicker ⁹⁴, F. Schlepfer ⁹⁴, A. Schmah⁹⁷, C. Schmidt ⁹⁷, H.R. Schmidt⁹³, M.O. Schmidt ³³, M. Schmidt⁹³, N.V. Schmidt ⁸⁷, A.R. Schmier ¹²¹, R. Schotter ¹²⁸, A. Schröter ³⁹, J. Schukraft ³³, K. Schweda ⁹⁷, G. Scioli ²⁶, E. Scomparin ⁵⁶, J.E. Seger ¹⁵, Y. Sekiguchi¹²³, D. Sekihata ¹²³, M. Selina ⁸⁴, I. Selyuzhenkov ⁹⁷, S. Senyukov ¹²⁸, J.J. Seo ^{94,58}, D. Serebryakov ¹⁴², L. Šerkšnytė ⁹⁵, A. Sevcenco ⁶³, T.J. Shaba ⁶⁸, A. Shabetai ¹⁰³, R. Shahoyan³³, A. Shangaraev ¹⁴², A. Sharma⁹⁰, B. Sharma ⁹¹, D. Sharma ⁴⁷, H. Sharma ⁵⁴, M. Sharma ⁹¹, S. Sharma ⁷⁶, S. Sharma ⁹¹, U. Sharma ⁹¹, A. Shatat ¹³⁰, O. Sheibani¹¹⁵, K. Shigaki ⁹², M. Shimomura⁷⁷, J. Shin¹², S. Shirinkin ¹⁴², Q. Shou ⁴⁰, Y. Sibirjak ¹⁴², S. Siddhanta ⁵², T. Siemiarczuk ⁷⁹, T.F. Silva ¹¹⁰, D. Silvermyr ⁷⁵, T. Simantathammakul¹⁰⁵, R. Simeonov ³⁷, B. Singh⁹¹, B. Singh ⁹⁵, K. Singh ⁴⁸, R. Singh ⁸⁰, R. Singh ⁹¹, R. Singh ⁴⁸, S. Singh ¹⁶, V.K. Singh ¹³⁴, V. Singhal ¹³⁴, T. Sinha ⁹⁹, B. Sitar ¹³, M. Sitta ^{132,56}, T.B. Skaali²⁰, G. Skorodumovs ⁹⁴, M. Slupecki ⁴⁴, N. Smirnov ¹³⁹, R.J.M. Snellings ⁵⁹, E.H. Solheim ²⁰, J. Song ¹⁷, C. Sonnabend ^{33,97}, F. Soramel ²⁸, A.B. Soto-hernandez ⁸⁸, R. Spijkers ⁸⁴, I. Sputowska ¹⁰⁷, J. Staa ⁷⁵, J. Stachel ⁹⁴, I. Stan ⁶³, P.J. Steffanic ¹²¹, S.F. Stiefelmaier ⁹⁴, D. Stocco ¹⁰³, I. Storehaug ²⁰, P. Stratmann ¹³⁷, S. Strazzi ²⁶, A. Sturniolo ^{31,53}, C.P. Stylianidis⁸⁴, A.A.P. Suaide ¹¹⁰, C. Suire ¹³⁰, M. Sukhanov ¹⁴², M. Suljic ³³, R. Sultanov ¹⁴², V. Sumberia ⁹¹, S. Sumowidagdo ⁸², S. Swain⁶¹, I. Szarka ¹³, M. Szymkowski ¹³⁵, S.F. Taghavi ⁹⁵, G. Taillepied ⁹⁷, J. Takahashi ¹¹¹, G.J. Tambave ⁸⁰, S. Tang ⁶, Z. Tang ¹¹⁹, J.D. Tapia Takaki ¹¹⁷, N. Tapus¹²⁵, L.A. Tarasovicova ¹³⁷, M.G. Tarzila ⁴⁶, G.F. Tassielli ³², A. Tauro ³³, G. Tejada Muñoz ⁴⁵, A. Telesca ³³, L. Terlizzi ²⁵, C. Terrevoli ¹¹⁵, S. Thakur ⁴, D. Thomas ¹⁰⁸, A. Tikhonov ¹⁴², N. Tiltmann ^{33,137}, A.R. Timmins ¹¹⁵, M. Tkacik¹⁰⁶, T. Tkacik ¹⁰⁶, A. Toia ⁶⁴, R. Tokumoto⁹², K. Tomohiro⁹², N. Topilskaya ¹⁴², M. Toppi ⁴⁹, T. Tork ¹³⁰, P.V. Torres⁶⁵, V.V. Torres ¹⁰³, A.G. Torres Ramos ³², A. Trifiro ^{31,53}, A.S. Triolo ^{33,31,53}, S. Tripathy ⁵¹, T. Tripathy ⁴⁷, S. Trogolo ³³, V. Trubnikov ³, W.H. Trzaska ¹¹⁶, T.P. Trzcinski ¹³⁵, A. Tumkin ¹⁴², R. Turrisi ⁵⁴, T.S. Tveter ²⁰, K. Ullaland ²¹, B. Ulukutlu ⁹⁵, A. Uras ¹²⁷, G.L. Usai ²³, M. Vala³⁸, N. Valle ²², L.V.R. van Doremalen⁵⁹, M. van Leeuwen ⁸⁴, C.A. van Veen ⁹⁴, R.J.G. van Weelden ⁸⁴, P. Vande Vyvre ³³, D. Varga ¹³⁸, Z. Varga ¹³⁸, M. Vasileiou ⁷⁸, A. Vasiliev ¹⁴², O. Vázquez Doce ⁴⁹, O. Vazquez Rueda ¹¹⁵, V. Vechemin ¹⁴², E. Vercellin ²⁵, S. Vergara Limón⁴⁵, R. Verma⁴⁷, L. Vermunt ⁹⁷, R. Vértesi ¹³⁸, M. Verweij ⁵⁹, L. Vickovic³⁴, Z. Vilakazi¹²², O. Villalobos Baillie ¹⁰⁰, A. Villani ²⁴, A. Vinogradov ¹⁴², T. Virgili ²⁹, M.M.O. Virta ¹¹⁶, V. Vislavicius⁷⁵, A. Vodopyanov ¹⁴³, B. Volkel ³³, M.A. Völkl ⁹⁴, K. Voloshin¹⁴², S.A. Voloshin ¹³⁶, G. Volpe ³², B. von Haller ³³, I. Vorobyev ⁹⁵, N. Vozniuk ¹⁴², J. Vrláková ³⁸, J. Wan⁴⁰, C. Wang ⁴⁰, D. Wang⁴⁰, Y. Wang ⁴⁰, Y. Wang ⁶, A. Wegrzynek ³³, F.T. Weiglhofer³⁹, S.C. Wenzel ³³, J.P. Wessels ¹³⁷, S.L. Weyhmiller ¹³⁹, J. Wiechula ⁶⁴, J. Wikne ²⁰, G. Wilk ⁷⁹, J. Wilkinson ⁹⁷, G.A. Willems ¹³⁷, B. Windelband ⁹⁴, M. Winn ¹²⁹, J.R. Wright ¹⁰⁸, W. Wu⁴⁰, Y. Wu ¹¹⁹, R. Xu ⁶, A. Yadav ⁴³, A.K. Yadav ¹³⁴,

S. Yalcin ⁷², Y. Yamaguchi ⁹², S. Yang²¹, S. Yano ⁹², Z. Yin ⁶, I.-K. Yoo ¹⁷, J.H. Yoon ⁵⁸, H. Yu¹², S. Yuan²¹, A. Yuncu ⁹⁴, V. Zaccolo ²⁴, C. Zampolli ³³, F. Zanone ⁹⁴, N. Zardoshti ³³, A. Zarochentsev ¹⁴², P. Závada ⁶², N. Zaviyalov¹⁴², M. Zhalov ¹⁴², B. Zhang ⁶, C. Zhang ¹²⁹, L. Zhang ⁴⁰, S. Zhang ⁴⁰, X. Zhang ⁶, Y. Zhang¹¹⁹, Z. Zhang ⁶, M. Zhao ¹⁰, V. Zhrebchevskii ¹⁴², Y. Zhi¹⁰, D. Zhou ⁶, Y. Zhou ⁸³, J. Zhu ^{97,6}, Y. Zhu⁶, S.C. Zugravel ⁵⁶, N. Zurlo ^{133,55}

Affiliation Notes

^I Also at: Max-Planck-Institut für Physik, Munich, Germany

^{II} Also at: Italian National Agency for New Technologies, Energy and Sustainable Economic Development (ENEA), Bologna, Italy

^{III} Also at: Dipartimento DET del Politecnico di Torino, Turin, Italy

^{IV} Also at: Department of Applied Physics, Aligarh Muslim University, Aligarh, India

^V Also at: Institute of Theoretical Physics, University of Wrocław, Poland

^{VI} Also at: An institution covered by a cooperation agreement with CERN

Collaboration Institutes

¹ A.I. Alikhanyan National Science Laboratory (Yerevan Physics Institute) Foundation, Yerevan, Armenia

² AGH University of Krakow, Cracow, Poland

³ Bogolyubov Institute for Theoretical Physics, National Academy of Sciences of Ukraine, Kiev, Ukraine

⁴ Bose Institute, Department of Physics and Centre for Astroparticle Physics and Space Science (CAPSS), Kolkata, India

⁵ California Polytechnic State University, San Luis Obispo, California, United States

⁶ Central China Normal University, Wuhan, China

⁷ Centro de Aplicaciones Tecnológicas y Desarrollo Nuclear (CEADEN), Havana, Cuba

⁸ Centro de Investigación y de Estudios Avanzados (CINVESTAV), Mexico City and Mérida, Mexico

⁹ Chicago State University, Chicago, Illinois, United States

¹⁰ China Institute of Atomic Energy, Beijing, China

¹¹ China University of Geosciences, Wuhan, China

¹² Chungbuk National University, Cheongju, Republic of Korea

¹³ Comenius University Bratislava, Faculty of Mathematics, Physics and Informatics, Bratislava, Slovak Republic

¹⁴ COMSATS University Islamabad, Islamabad, Pakistan

¹⁵ Creighton University, Omaha, Nebraska, United States

¹⁶ Department of Physics, Aligarh Muslim University, Aligarh, India

¹⁷ Department of Physics, Pusan National University, Pusan, Republic of Korea

¹⁸ Department of Physics, Sejong University, Seoul, Republic of Korea

¹⁹ Department of Physics, University of California, Berkeley, California, United States

²⁰ Department of Physics, University of Oslo, Oslo, Norway

²¹ Department of Physics and Technology, University of Bergen, Bergen, Norway

²² Dipartimento di Fisica, Università di Pavia, Pavia, Italy

²³ Dipartimento di Fisica dell'Università and Sezione INFN, Cagliari, Italy

²⁴ Dipartimento di Fisica dell'Università and Sezione INFN, Trieste, Italy

²⁵ Dipartimento di Fisica dell'Università and Sezione INFN, Turin, Italy

²⁶ Dipartimento di Fisica e Astronomia dell'Università and Sezione INFN, Bologna, Italy

²⁷ Dipartimento di Fisica e Astronomia dell'Università and Sezione INFN, Catania, Italy

²⁸ Dipartimento di Fisica e Astronomia dell'Università and Sezione INFN, Padova, Italy

²⁹ Dipartimento di Fisica 'E.R. Caianiello' dell'Università and Gruppo Collegato INFN, Salerno, Italy

³⁰ Dipartimento DISAT del Politecnico and Sezione INFN, Turin, Italy

³¹ Dipartimento di Scienze MIFT, Università di Messina, Messina, Italy

³² Dipartimento Interateneo di Fisica 'M. Merlin' and Sezione INFN, Bari, Italy

³³ European Organization for Nuclear Research (CERN), Geneva, Switzerland

³⁴ Faculty of Electrical Engineering, Mechanical Engineering and Naval Architecture, University of Split, Split, Croatia

³⁵ Faculty of Engineering and Science, Western Norway University of Applied Sciences, Bergen, Norway

- ³⁶ Faculty of Nuclear Sciences and Physical Engineering, Czech Technical University in Prague, Prague, Czech Republic
- ³⁷ Faculty of Physics, Sofia University, Sofia, Bulgaria
- ³⁸ Faculty of Science, P.J. Šafárik University, Košice, Slovak Republic
- ³⁹ Frankfurt Institute for Advanced Studies, Johann Wolfgang Goethe-Universität Frankfurt, Frankfurt, Germany
- ⁴⁰ Fudan University, Shanghai, China
- ⁴¹ Gangneung-Wonju National University, Gangneung, Republic of Korea
- ⁴² Gauhati University, Department of Physics, Guwahati, India
- ⁴³ Helmholtz-Institut für Strahlen- und Kernphysik, Rheinische Friedrich-Wilhelms-Universität Bonn, Bonn, Germany
- ⁴⁴ Helsinki Institute of Physics (HIP), Helsinki, Finland
- ⁴⁵ High Energy Physics Group, Universidad Autónoma de Puebla, Puebla, Mexico
- ⁴⁶ Horia Hulubei National Institute of Physics and Nuclear Engineering, Bucharest, Romania
- ⁴⁷ Indian Institute of Technology Bombay (IIT), Mumbai, India
- ⁴⁸ Indian Institute of Technology Indore, Indore, India
- ⁴⁹ INFN, Laboratori Nazionali di Frascati, Frascati, Italy
- ⁵⁰ INFN, Sezione di Bari, Bari, Italy
- ⁵¹ INFN, Sezione di Bologna, Bologna, Italy
- ⁵² INFN, Sezione di Cagliari, Cagliari, Italy
- ⁵³ INFN, Sezione di Catania, Catania, Italy
- ⁵⁴ INFN, Sezione di Padova, Padova, Italy
- ⁵⁵ INFN, Sezione di Pavia, Pavia, Italy
- ⁵⁶ INFN, Sezione di Torino, Turin, Italy
- ⁵⁷ INFN, Sezione di Trieste, Trieste, Italy
- ⁵⁸ Inha University, Incheon, Republic of Korea
- ⁵⁹ Institute for Gravitational and Subatomic Physics (GRASP), Utrecht University/Nikhef, Utrecht, Netherlands
- ⁶⁰ Institute of Experimental Physics, Slovak Academy of Sciences, Košice, Slovak Republic
- ⁶¹ Institute of Physics, Homi Bhabha National Institute, Bhubaneswar, India
- ⁶² Institute of Physics of the Czech Academy of Sciences, Prague, Czech Republic
- ⁶³ Institute of Space Science (ISS), Bucharest, Romania
- ⁶⁴ Institut für Kernphysik, Johann Wolfgang Goethe-Universität Frankfurt, Frankfurt, Germany
- ⁶⁵ Instituto de Ciencias Nucleares, Universidad Nacional Autónoma de México, Mexico City, Mexico
- ⁶⁶ Instituto de Física, Universidade Federal do Rio Grande do Sul (UFRGS), Porto Alegre, Brazil
- ⁶⁷ Instituto de Física, Universidad Nacional Autónoma de México, Mexico City, Mexico
- ⁶⁸ iThemba LABS, National Research Foundation, Somerset West, South Africa
- ⁶⁹ Jeonbuk National University, Jeonju, Republic of Korea
- ⁷⁰ Johann-Wolfgang-Goethe Universität Frankfurt Institut für Informatik, Fachbereich Informatik und Mathematik, Frankfurt, Germany
- ⁷¹ Korea Institute of Science and Technology Information, Daejeon, Republic of Korea
- ⁷² KTO Karatay University, Konya, Turkey
- ⁷³ Laboratoire de Physique Subatomique et de Cosmologie, Université Grenoble-Alpes, CNRS-IN2P3, Grenoble, France
- ⁷⁴ Lawrence Berkeley National Laboratory, Berkeley, California, United States
- ⁷⁵ Lund University Department of Physics, Division of Particle Physics, Lund, Sweden
- ⁷⁶ Nagasaki Institute of Applied Science, Nagasaki, Japan
- ⁷⁷ Nara Women's University (NWU), Nara, Japan
- ⁷⁸ National and Kapodistrian University of Athens, School of Science, Department of Physics, Athens, Greece
- ⁷⁹ National Centre for Nuclear Research, Warsaw, Poland
- ⁸⁰ National Institute of Science Education and Research, Homi Bhabha National Institute, Jatni, India
- ⁸¹ National Nuclear Research Center, Baku, Azerbaijan
- ⁸² National Research and Innovation Agency - BRIN, Jakarta, Indonesia
- ⁸³ Niels Bohr Institute, University of Copenhagen, Copenhagen, Denmark
- ⁸⁴ Nikhef, National institute for subatomic physics, Amsterdam, Netherlands
- ⁸⁵ Nuclear Physics Group, STFC Daresbury Laboratory, Daresbury, United Kingdom
- ⁸⁶ Nuclear Physics Institute of the Czech Academy of Sciences, Husinec-Řež, Czech Republic
- ⁸⁷ Oak Ridge National Laboratory, Oak Ridge, Tennessee, United States

- ⁸⁸ Ohio State University, Columbus, Ohio, United States
⁸⁹ Physics department, Faculty of science, University of Zagreb, Zagreb, Croatia
⁹⁰ Physics Department, Panjab University, Chandigarh, India
⁹¹ Physics Department, University of Jammu, Jammu, India
⁹² Physics Program and International Institute for Sustainability with Knotted Chiral Meta Matter (SKCM2), Hiroshima University, Hiroshima, Japan
⁹³ Physikalisches Institut, Eberhard-Karls-Universität Tübingen, Tübingen, Germany
⁹⁴ Physikalisches Institut, Ruprecht-Karls-Universität Heidelberg, Heidelberg, Germany
⁹⁵ Physik Department, Technische Universität München, Munich, Germany
⁹⁶ Politecnico di Bari and Sezione INFN, Bari, Italy
⁹⁷ Research Division and ExtreMe Matter Institute EMMI, GSI Helmholtzzentrum für Schwerionenforschung GmbH, Darmstadt, Germany
⁹⁸ Saga University, Saga, Japan
⁹⁹ Saha Institute of Nuclear Physics, Homi Bhabha National Institute, Kolkata, India
¹⁰⁰ School of Physics and Astronomy, University of Birmingham, Birmingham, United Kingdom
¹⁰¹ Sección Física, Departamento de Ciencias, Pontificia Universidad Católica del Perú, Lima, Peru
¹⁰² Stefan Meyer Institut für Subatomare Physik (SMI), Vienna, Austria
¹⁰³ SUBATECH, IMT Atlantique, Nantes Université, CNRS-IN2P3, Nantes, France
¹⁰⁴ Sungkyunkwan University, Suwon City, Republic of Korea
¹⁰⁵ Suranaree University of Technology, Nakhon Ratchasima, Thailand
¹⁰⁶ Technical University of Košice, Košice, Slovak Republic
¹⁰⁷ The Henryk Niewodniczanski Institute of Nuclear Physics, Polish Academy of Sciences, Cracow, Poland
¹⁰⁸ The University of Texas at Austin, Austin, Texas, United States
¹⁰⁹ Universidad Autónoma de Sinaloa, Culiacán, Mexico
¹¹⁰ Universidade de São Paulo (USP), São Paulo, Brazil
¹¹¹ Universidade Estadual de Campinas (UNICAMP), Campinas, Brazil
¹¹² Universidade Federal do ABC, Santo Andre, Brazil
¹¹³ University of Cape Town, Cape Town, South Africa
¹¹⁴ University of Derby, Derby, United Kingdom
¹¹⁵ University of Houston, Houston, Texas, United States
¹¹⁶ University of Jyväskylä, Jyväskylä, Finland
¹¹⁷ University of Kansas, Lawrence, Kansas, United States
¹¹⁸ University of Liverpool, Liverpool, United Kingdom
¹¹⁹ University of Science and Technology of China, Hefei, China
¹²⁰ University of South-Eastern Norway, Kongsberg, Norway
¹²¹ University of Tennessee, Knoxville, Tennessee, United States
¹²² University of the Witwatersrand, Johannesburg, South Africa
¹²³ University of Tokyo, Tokyo, Japan
¹²⁴ University of Tsukuba, Tsukuba, Japan
¹²⁵ University Politehnica of Bucharest, Bucharest, Romania
¹²⁶ Université Clermont Auvergne, CNRS/IN2P3, LPC, Clermont-Ferrand, France
¹²⁷ Université de Lyon, CNRS/IN2P3, Institut de Physique des 2 Infinis de Lyon, Lyon, France
¹²⁸ Université de Strasbourg, CNRS, IPHC UMR 7178, F-67000 Strasbourg, France, Strasbourg, France
¹²⁹ Université Paris-Saclay, Centre d’Etudes de Saclay (CEA), IRFU, Département de Physique Nucléaire (DPhN), Saclay, France
¹³⁰ Université Paris-Saclay, CNRS/IN2P3, IJCLab, Orsay, France
¹³¹ Università degli Studi di Foggia, Foggia, Italy
¹³² Università del Piemonte Orientale, Vercelli, Italy
¹³³ Università di Brescia, Brescia, Italy
¹³⁴ Variable Energy Cyclotron Centre, Homi Bhabha National Institute, Kolkata, India
¹³⁵ Warsaw University of Technology, Warsaw, Poland
¹³⁶ Wayne State University, Detroit, Michigan, United States
¹³⁷ Westfälische Wilhelms-Universität Münster, Institut für Kernphysik, Münster, Germany
¹³⁸ Wigner Research Centre for Physics, Budapest, Hungary
¹³⁹ Yale University, New Haven, Connecticut, United States
¹⁴⁰ Yonsei University, Seoul, Republic of Korea

¹⁴¹ Zentrum für Technologie und Transfer (ZTT), Worms, Germany

¹⁴² Affiliated with an institute covered by a cooperation agreement with CERN

¹⁴³ Affiliated with an international laboratory covered by a cooperation agreement with CERN.